BIOMETRIC RECOGNITION

A THESIS

SUBMITTED TO THE DELHI TECHNOLOGICAL UNIVERSITY

FOR THE AWARD OF THE DEGREE OF

DOCTOR OF PHILOSOPHY

IN

ELECTRONICS & COMMUNICATION ENGINEERING

SUBMITTED BY

AJAI KUMAR GAUTAM

(Roll No. 2K11/PhD/EC/08)

Under the Guidance of
Prof. Rajiv Kapoor

DEPARTMENT OF ELECTRONICS & COMMUNICATION ENGINEERING

DELHI TECHNOLOGICAL UNIVERSITY

(Formerly Delhi College of Engineering)

DELHI- 110042 (INDIA)

MAY -2022

BIOMETRIC RECOGNITION

A THESIS

SUBMITTED TO THE DELHI TECHNOLOGICAL UNIVERSITY

FOR THE AWARD OF THE DEGREE OF

DOCTOR OF PHILOSOPHY

IN

ELECTRONICS & COMMUNICATION ENGINEERING

SUBMITTED BY

AJAI KUMAR GAUTAM

(Roll No. 2K11/PhD/EC/08)

Under the Guidance of
Prof. Rajiv Kapoor

DEPARTMENT OF ELECTRONICS & COMMUNICATION ENGINEERING

DELHI TECHNOLOGICAL UNIVERSITY

(Formerly Delhi College of Engineering)

DELHI- 110042 (INDIA)

MAY -2022

CERTIFICATE

This is to certify that the thesis entitled "**Biometric Recognition**" being submitted by **Mr. Ajai Kumar Gautam (Reg No: 2K11/PhD/EC/08)** for the award of degree of Doctor of Philosophy to the Delhi Technological University is based on the original work carried out by him. He has worked under my supervision and has fulfilled the requirements, which to my knowledge have reached the requisite standard for the submission of this thesis. It is further certified that the work embodied in this thesis has neither partially nor fully submitted to any other university nor institution for the award of any degree or diploma.

Prof. Rajiv Kapoor
(Supervisor)
Department of Electronics & Communication Engineering
Delhi Technological University, Delhi

ACKNOWLEDGMENTS

I'm in debt and would like to express a great feeling of gratitude toward several people who guided and supported me throughout the completion of my research program.

First and foremost, I would like to thank my supervisor, **Prof. Rajiv Kapoor**, for his support and faith in me during the course of my Ph.D. Studies. My research work cannot be turned into a prodigious experience without his substantial and thorough approach, together with his unpretentious interest in the research subject.

Above all, my deepest thanks go to my parents for their absolute affection and support. Also, my wholehearted recognition to my wife (**Anita**), my daughter (**Aashi**), and my son (**Aarush**) for their love, affection, patience, and everyday devotion that made it possible to complete this research work.

Finally, but not lastly, I would also like to express my sincere thanks to all those who supported me directly and indirectly along with my colleagues (especially **Prof. Rajesh Birok** & **Prof Vinod Kumar)** for their encouragement and advice, which they provided me during this research journey.

ABSTRACT

Biometric Recognition is the essential process of authenticating an individual and has a very wide application area starting from one's essential need like phone or laptop access to high end applications like in, Airport, Border control, surveillance, forensic applications etc. It is implemented almost in every system that require some sort of authentication for establishing the identity of a person. Biometrics recognition is based on the Biometric traits, which are the physical or behavioral characteristics of a person that are physically or behaviorally linked to the person. Since Biometric traits are physically linked to the user therefore very difficult to steal or forge and person do not require to remember the login or password for accessing any system or premises.

There are various biometric traits like Face, Finger Print, Finger veins, Iris, Scalera, etc which are extensively utilized in several recognition applications. Some recognition applications use number of traits of a person to have high recognition accuracy. Some even take physical as well as behavioral along with soft biometric traits like hand shape etc. to have robust recognition system that works in unconstrained environment with higher accuracy.

Purpose of this research work is to improve the accuracy of the recognition system by taking number of traits of a person together called Multi-Modal Biometric (MMB) Recognition and by focusing on the finger vein trait, which is one of the current research areas as it can be captured only of a live person.

A new method is proposed, the MMB recognition system centered on the Features Level and Scores Level (FLSL) fusion method and Modified Deep Learning Neural Network (MDLNN) classifier in order to enhance the performance. The face, ear, retina, fingerprint, and front hand image traits are considered by the proposed method.

The unique patterns of finger veins (FV) are utilized by Finger vein recognition (FVR) for detecting individuals at a high-level accuracy. However, on account of the existence of artifacts, irregular shading, distortions, etc, precise FV detection is a difficult task. A framework for identifying FV is created by the work to offer a precise biometric authorization utilizing Enhanced Sigmoid Reweighted based Convolutional Neural Network (ES-RwCNN).

LIST OF PUBLICATIONS

Ajai Kumar Gautam & Rajiv Kapoor "*Multi-modal biometric recognition system based on FLSL fusion method and MDLNN classifier*." Turkish Journal of Computer and Mathematics Education, ISSN: 2382-2389 in Volume 12, No. 11 (2021). [SJR-0.218] [Published in SCOPUS INDEXED JOURNAL]

Ajai Kumar Gautam & Rajiv Kapoor "*A Novel ES-RwCNN Based Finger Vein Recognition System with Effective L_{12} DTP Descriptor and AWM-WOA Selection*", Engineering Letters, vol. 30, no.2, pp882-891, 2022. Journal ISSN: 1816-093X / 1816-0948 [SJR-0.265] [ESCI]

Ajai Kumar Gautam & Rajiv Kapoor "*A review on Finger vein-based Recognition*" published in 2021 IEEE 8th Uttar Pradesh Section International Conference on Electrical, Electronics and Computer Engineering (UPCON); DOI 10.1109/UPCON52273.2021.9667572

Abhishek & **Ajai Kumar Gautam** "*Study on enhancing the accuracy of fingerprint recognition system*", published in book "Recent Trends in Communication and Electronics" 2021 CRC Press, Taylor Francis Group eBook ISBN9781003193838.

Aryan Singh, Hardik Goyal, Amar & **Ajai Kumar Gautam** "*Human Identification Based on Hand Dorsal Vein Pattern using BRISK & SURF Algorithm*, ISSN: 2249 – 8958, Volume-9 Issue-4, April, 2020 [Published in SCOPUS INDEXED JOURNAL]

TABLE OF CONTENTS

LIST OF FIGURES

LIST OF TABLES

List of Abbreviations

MMB	Multimodal Biometric
ECG	Electrocardiogram
EEG	Electroencephalogram
DNA	Deoxyribonucleic acid
IPHE	Improved Plateau Histogram Equalization
PPWS	Penalty and Pearson correlation-based Watershed Segmentation
MDLNN	Modified Deep Learning Neural Network
ES-RwCNN	Enhanced Sigmoid Reweighted based Convolutional Neural Network
TMF-CLAHE	Trapezoid Membership Function-Based Contrast Limited Adaptive Histogram Equalization
CE	Contrast Enhancement
AWM-WOA	Adaptive Weight Mutated Whale Optimization Algorithm
CC	Computational Complexity
FVR	Finger Vein Recognition
RLF	Rank-Level Fusions
SLF	Score Level Fusions
NN	Neural Network
CNN	Convolutional NN
L-CNN	Lightweight CNN
CA	Classification Accuracy
RR	Recognition Rate
SDH	Supervised Discrete Hashing
FVRAS-Net	FVR and Anti Spoofing Network
LSR	Least Square Regression
NVP	Non- Vein Points
PCNN	Pulse Coupled Neural Network
ELM	Extreme Learning Machine
GCNN	Graph Convolutional Neural networks
G-SLGS	Symmetric Local Graph Structure

AHE	Adaptive Histogram Equalization
CLAHE	Contrast Limited Adaptive Histogram Equalization
PDV	Pixel Difference Value
AMBP	Anchor Based Manifold Binary Pattern
LBP	Local Binary Pattern
WLD	Wide Line Detector
PHE	Plateau Histogram Equalization
WS	Watershed Segmentation
KLDA	Kernelized Linear Discriminants Analysis

CHAPTER 1

BIOMETRIC RECOGNITION: AN INTRODUCTION

Firstly, Biometric Recognition is explained briefly. Followed by the general process of enrollment, identification, and verification in a biometric recognition system is explained. Unimodal and multi-modal Biometric recognition systems are explained. Followed by a brief explanation of some of the most extensively used biometric traits. Thereafter the challenges in the multi-modal biometric recognition system, and in particular the finger vein biometric recognition system, are explained. Finally, the problem statement is defined along with the contribution of this thesis, followed by the significance of this research work and an overview of the whole thesis.

1.1 Biometric Recognition

In a variety of applications, the system requires a personal recognition scheme so that it can be ensured that only the legitimate or authorized user/person is accessing the resources. The application ranges from access to important buildings such as airports, access to the laptop, mobile phones to ATMs. Biometric recognition is one such scheme [1]. Biometric recognition of a person means recognizing a person based on his/her traits that are physically linked to the user, or we can say that the user possesses these traits naturally. These traits are often referred to as Biometric traits.

Based on these biometric traits recognition process is performed by an automated system that keeps a record of the biometric traits of the enrolled persons. Usually, some features from the biometric traits are extracted. These extracted features are called templates. This template is stored in some system that creates a database of users. This whole process of storing the template of each user is known as the enrollment process.

The enrollment process is a continuous process as the new users are enrolled. Not all physiological traits can be used as biometric traits; only those that have some basic properties that can be measured by some sensors can be recorded on some systems and can be quantified. Further to be more precise these biometric traits should have the qualities [2] like – *Universality* means it is available with every person, *Distinctiveness* means it is different for each person, no two or more person have similar traits, *Permanence* means it remains almost same in the person over irrespective of age advances, *Collectability* means these traits can be measured or quantified. In addition to these, there are other issues that need to be taken care of when considering a Biometric recognition system for authenticating users; these are – *Performance*, i.e., required recognition rate and accuracy, *Acceptability*, how much peoples or users are ready or comfortable to provide the biometric trait for authentication. *Circumvention* means how difficult to crack this authentication/ recognition system by the imposter.

A real-time Biometric recognition system must have high accuracy and high computation speed, must be cost-effective, must be robust to deter any imposter representations, and overall it should be safe for the environment and the users.

The method of recognizing a person centered on one's unique physiological or behavioral attributes is called Biometrics [3]. The method of biometric recognition offers various advantages over the conventional techniques of recognizing a person. One of the many advantages is the fact that these biometric traits are difficult to be copied, and in some cases, the person is required to be physically present to be recognized. Therefore, this not only restricts unauthorized access but also ensures the liveliness of a person.

1.2 Multimodal Biometric (MMB) Systems:

Various biometric traits are used for real-time recognition. The most commonly used biometric traits are iris, face, and fingerprint. In some applications, more than one biometric trait is used to achieve higher accuracy or recognition rate. Such systems are known as multimodal biometric systems [4].

A Biometric Recognition (BR) system can be considered as an autonomous pattern recognition system that recognizes the user by authenticating his/her biometric traits. Either the user presents these biometric traits itself to access a resource, or it is acquired by the system, and the user is not aware of this. For e.g., in a video surveillance application, face images are captured to recognize a particular person. The Biometric enrollment process is shown in Figure 1.1

A biometric system may operate either in verification (authentication) mode or in an identification mode. In verification, the person claimed identity is either accepted or rejected, i.e., it is a 1:1 matching problem shown in figure 1.2, whereas in identification, A biometric system must be able to identify a person by by comparing its biometric traits with the stored traits of people. Therefore, it involves a 1: N matching problem as shown in figure 1.3, and it is more challenging than the verification.

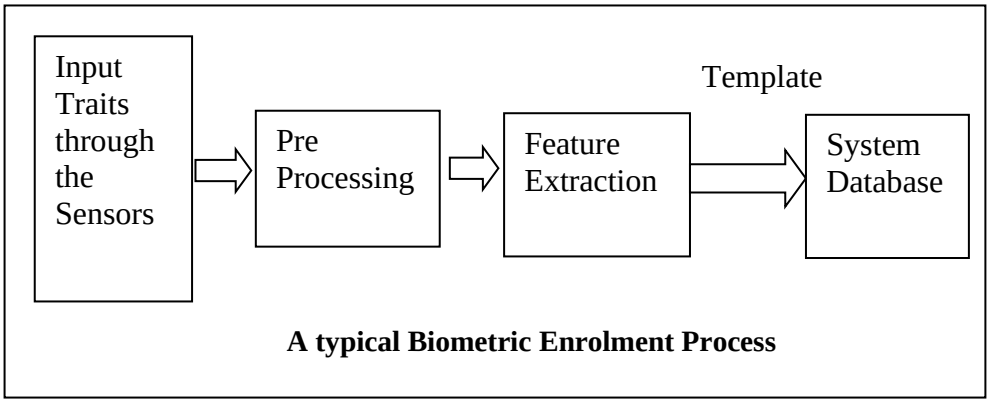

Figure 1.1: A typical Biometric Enrolment Process is shown

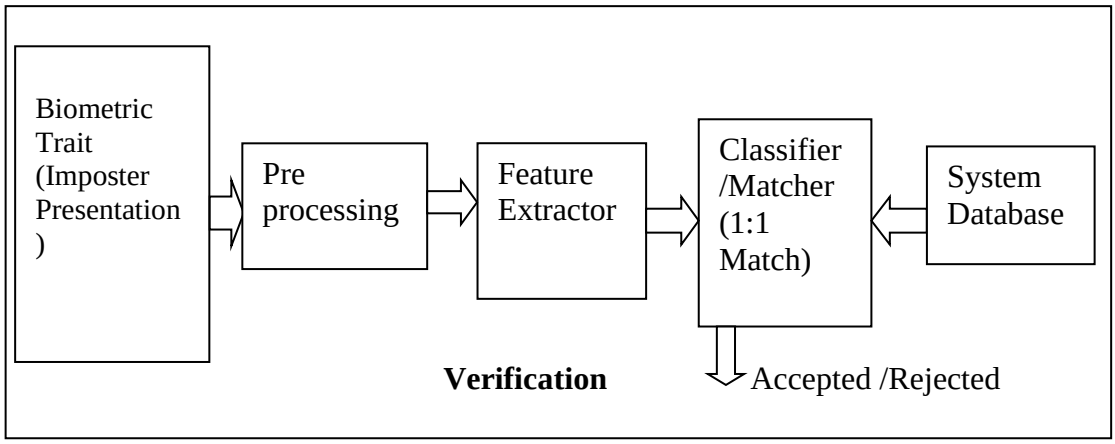

Figure 1.2: A typical Biometric Identification or verification Process

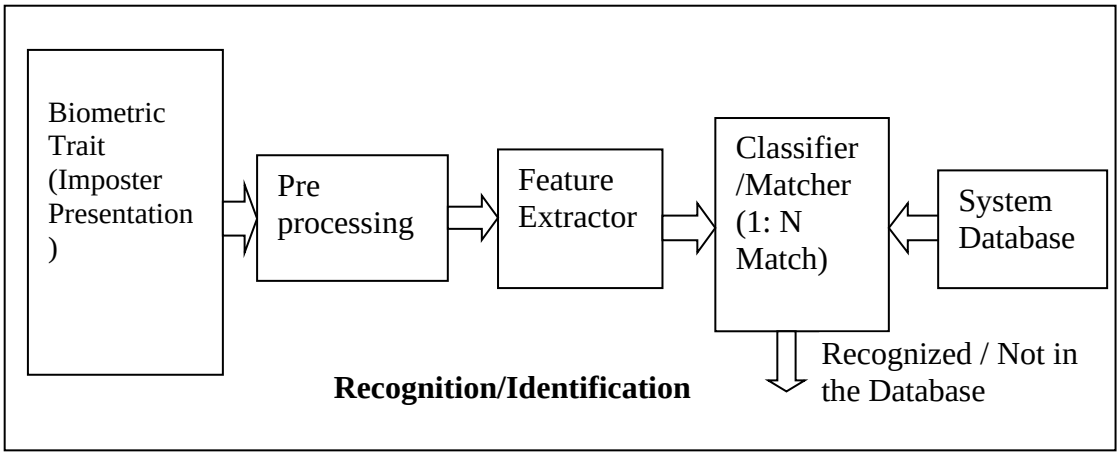

Figure 1.3: A typical Biometric recognition or authentication process is shown

1.3 Biometric Traits

The various biometric traits of a person can be classified into two broad categories:

a. **Based on the physiological characteristics**: - Fingerprints which have been used for more than100 years, Palm prints, Hand geometry, Hand veins, Finger veins, Iris recognition, Retina scan, Sclera recognition, Ear canal, Face recognition, Facial

thermo-gram, ECG, EEG, and DNA.

b. **Based on the behavioral characteristics**: - Keystroke, Signature, Voice, Gait, and Mouse Gesture Dynamics.

Let us look briefly at the different biometric traits and their features that are utilized in the different applications where the user or person authentication is required.

Finger print: - Finger print Biometrics have been used for a very long time though initially, it is used in forensic application to establish whether the person is physically present at a particular crime scene or not. This is done by lifting the fingerprint from the scene and matching it with the available dataset and the prime suspect's fingerprints. Finger prints are unique to each and every individual. They are universally accepted by all. The most visible features in finger print are ridge patterns and valley points or patterns. One major drawback with this trait is that they are computation-intensive, and further, the fingerprint of labor or the workforce suffers from many distortions such as cuts and bruises, and that changes with time.

Palm prints: Palm print covers a wider part of the hand and has more texture and structural features such as principle palm lines, wrinkles, shape, ridge, valley, etc. Palm print suffers from some issues that come during capture stages, such as position and direction during capturing. Stretching of the palm, rotational, and translation issues. In this first, ROI is extracted from where the various features are taken out to establish the identity of the user.

Hand geometry: has an advantage; its structure remains stable and does not vary with time [5]. It has universality property and invariance property; however, it lacks the

property of best distinctiveness. Nowadays, a focus is on the 3-D hand geometry as a biometric trait usually used along with some other biometric traits. A 3-D template is created from a 2-D template captured at different depths.

Hand veins: or Hand dorsal vein biometric[6] has advantages such that it can not be forged as it can be captured of a live person, not affected by surface impurities as it is scanned by an IR camera, and also the imaging environment does not affect its feature and hence recognition accuracy.

Finger veins: [7]this biometric trait has similar advantages as offered by the Hand dorsal vein, such that difficult to be forged or copied as its lies internal to the human body. Further, it provides many veins and non-veins features in a small area that can be used to establish and verify the identity of a person. Either one finger or multiple fingers can be used for the recognition process

Iris: Iris is the region that lies in between the pupil and the sclera; the sclera is the visible white region of the eye, while the pupil is the black region[8]. Iris biometric trait mainly uses NIR images[9] it is the most accurate and robust biometric trait. It remains stable over the long-time line. Some Iris recognition uses the Visible range spectrum images that have additional information but suffers from reflection-related problems that need additional processing.

Sclera: sclera is the visible white region of the eye, while the pupil is the black region [8] sclera consists of a vein pattern that can be used to authenticate a person. This can be captured by the camera operating in the visible range and, therefore, can be acquired from a distance. However, its vein structure is complex as it spreads in multilayers, is defocused and often has deformities that are nonlinear[10].

Retina scan: - This Biometric trait consists of a vascular structure that is also unique, remain stable for almost the whole life of a person[11] and can be captured of a live person. Usually, graph-based techniques are used to extract features. However, it suffers from the drawback that the vascular structure changes if a person is suffering from certain lifestyle-related diseases.

Ear: Ear biometrics has shape features and is also classified into helix representation and antihelix representation[12] which are unique and can be used to authenticate the user. This has the advantage that it remains stable throughout life. It is not affected by facial expression. Usually, the key points are detected in the ear, and that creates a template. This trait is computation-intensive though it can be captured from a distance.

Face: The initial biometric attributes to be utilised for authentication was the face. Features are taken either from the whole face or from the specific regions of the face[13]. These features are then used to match the features available in the database. Face can be taken from the video frames also and mostly used in various applications, including surveillance and forensic applications. Though it can be taken from a distance, however, it suffers from various constraints. Age also affects facial features over the time.

Facial Thermo-gram: in this case, an IR thermal image of the face is taken[14]. It has the advantage that illumination variation and facial state also do not affect the facial features. It also captures the vascular structure of the face. It can be used as a thermal image or identity of a person.

ECG: biometric trait used in the clinical medicine field to identify a person. ECG

signature is unique to a person and depends on the individual heart[15] its structure and physical built. Fiducial and non- fiducial points of ECG are used for recognition.

EEG: Electroencephalography [EEG] is the trait that is related to the brain activity of an individual. It can be measured by cost-effective instruments or systems. It has a high temporal resolution. It has some basic features as well as others, such as phase synchronization features[16] as well as it can be taken only from a live person. However, it suffers from some artifacts such as muscle contraction, active reference, etc., that need to be taken while designing an authentication system based on this trait.

DNA: Deoxyribonucleic acid (DNA) is the genetic code of an individual[2] and it is unique. However, identical twins have exactly the same DNA. It is widely used in forensic science to establish the identity of an individual at the crime scene. It, too, has a few limitations. They are highly sensitive and get distorted or contaminated easily; an automated system based on a real-time basis on this is difficult. It also involves some privacy concerns.

Keystroke: is a behavioral biometric trait. It is the way that a person types on a computer, laptop, etc. There are many approaches. One such approach can be grouped into two. One is based on the fixed text type- in which a person types a fixed set of characters; the other is a free text based[17]- in which the user types any character of his or her choice. Timing parameters can also be used along with keystroke dynamics. However, the typing behavior of a person itself varies. It also varies even with the new keyboard.

Signature: is the style that a person uses to write his or her name in a flow on a paper. It is used in Government documents, legal documents, and commercial, financial transactions

for authentication. A drawback with this trait is that it does not remain stable; it changes with time. It is affected by the emotional and physical state of a person. Forgery chances are more with this type of biometric trait. A large dataset is not available; however, synthetic databases are created to test this authentication[2], [18].

Voice: A Person's voice we normally use to recognize the person. It is the natural means of communication between the persons. The various feature can be extracted from voice, such as speech frequency, formant frequency, arithmetic mean, the average value of speech/voice in a frame, etc. It is unique to every individual and depends on the vocal cords and other physical attributes of the mouth and neck[2], [19]. It changes with the medical condition and age, and emotional state of the person.

Gait: is the person's walking style. The advantage of this biometric trait is that it can be captured from a distance even without the knowledge of the person therefore used in surveillance applications. Generally, videos are captured from which gait features are extracted, such as movements of different joints [2], [20]etc. This can be affected by the medical condition related to joint movement, clothing, capture view, etc. This is computationally taxing and requires a large set of inputs.

Mouse Gesture Dynamics: captures the mouse movement along with mouse click when the mouse is connected to a desktop. From this data, a biometric signature is extracted to authenticate a user. one of the primary advantages of this biometric is that it can be used continuously to authenticate a user in a session connected to a pc. However, it faces many challenges when used for static user authentication during the login time mouse[2], [20]. A sufficient amount of data needs to be captured to accurately authenticate a user, and it is a time-consuming process in real-time mode.

1.4 Challenges in Biometric Recognition:

Biometric recognition systems are designed while keeping the verification or identification accuracy as much as high with the constraints of lower computation cost, higher user convenience, higher security level, and minimum memory requirements. Non-universality, intra-class differences, data noise, spoof attempts, and uniqueness are all problems with the unimodal system [21]. One of the reasons that these issues arise is due to the user's poor interaction with the various sensor that captures biometric trait.

The vein pattern present beneath the skin of the finger is utilized in Finger Vein (FV) Recognition for authenticating a person. Though it provides good accuracy, it suffers from various artifacts like- irregular shading, distortions, vein deformation, etc.

Finger translation is also a major issue it is caused during capture stage. Two reasons are, one is in plane translation, and other one is out of plane rotation of complete finger. As a result, the finger has a different angle from the base line. The scale of finger translation in one place is bigger than in others. Temperature changes in the imaging environment, as well as muscle tension in the individual, can produce considerable elastic deformation of the vein pattern. In addition, FV recognition system accuracy is affected by the low-quality image regions

1.5 Problem statement

A new method is proposed using the different biometric traits in order to enhance the performance such as accuracy, based on the concept of a multi-modal Biometric (MMB) recognition system. An Improved Plateau Histogram Equalization (IPHE) algorithm is proposed to enhance all the inputted traits. A Penalty and Pearson correlation-based Watershed Segmentation (PPWS) algorithm is proposed to eliminate the unwanted

information in the ear and finger traits. Also, a Modified Deep Learning Neural Network (MDLNN) classifier is proposed in order to enhance the performance.

A new framework is proposed for identifying FV to offer a precise biometric authorization utilizing Enhanced Sigmoid Reweighted based Convolutional Neural Network (ES-RwCNN). A Trapezoid Membership Function-Based Contrast Limited Adaptive Histogram Equalization (TMF-CLAHE) is proposed for contrast enhancement (CE) that intensifies the image by evading irregular shading and vein posture deformation that improves the accuracy rate. Further, an Adaptive Weight Mutated Whale Optimization Algorithm (AWM-WOA) technique is proposed that enhances the proposed FV recognition accuracy and decreases the computational complexity (CC)

1.6 Main contribution of the Thesis

A new multi-modal Biometric recognition system is proposed with a different set of biometric traits, namely- face, ear, retina, fingerprint, and front hand image. These are enhanced by a new method of Contrast enhancement along with modified Deep Learning NN are proposed.

Further, to mitigate the effects of uneven shading along with vein posture deformation that degrades the FV authentication's accuracy, a new method for FV recognition is proposed that uses a new TMF-CLAHE enhancement method. Also, an Es-RwCNN is proposed for enhancing the classification accuracy (CA) for Finger Vein Recognition (FVR).

1.7 Significance of the Study

The finding of this research works confirms that the MMB system with improved plateau histogram equalization reduces the effects of over enhancement etc., and with a modified

Deep Learning Neural Network, recognition accuracy improves as well as the recognition becomes more robust.

This study also confirms that with the help of the new TMF-CLAHE method, the effects of different artifacts on the FV recognition can be reduced, and accuracy can be improved.

1.8 Thesis Overview

Chapter 2 covers the details of the research work carried out earlier, along with their pros and cons, challenges, issues, and approaches are described. It also states some of the research gaps in the concerned area, and based upon these research gaps, the objectives of the research are formulated.

Chapter 3 covers the details of the proposed method for MMB recognition using the FLSL fusion technique in detail with results and significant findings. Proposed Improved Plateau Histogram Equalization (IPHE) and modified Deep Learning Neural Network classifiers are discussed in detail.

Chapter 4 covers the details of the proposed method for the finger vein recognition system. TMF_CLAHE, Enhanced Sigmoid Reweighted based Convolutional Neural Network (ES-RwCNN), is also discussed in detail with results and significant findings.

Chapter 5 States the important conclusions drawn from this research and also includes details of the future scope of work.

CHAPTER 2

LITERATURE REVIEW

This chapter consists of details of the previous research work done in the field of MMB, Unimodal biometric, finger vein recognition system along with the issues, challenges. The research gaps and research objective are also given.

2.1 Multi-Modal Biometric Recognition

Biometric systems are utilized in multiple areas for recognition [22]. Besides different other factors, namely cost, convenience, security level, memory requirements, etc., the Biometric system is also centered upon its verification or identification accuracy[23]. Non-universality, intra-class differences, data noise, spoof threats, and individuality are all problems with the unimodal system. [21]. Due to the user's poor interaction with the sensor, these variations take place[24]. The usage of many biometric modalities (i.e., the combination between two or several different biometrics data or combining the physiological along with behavioral characteristics) within the same system is the solution for overcoming these shortcomings, which is named multiple biometric systems [25], [26]. Thus, greater attention to the Multi-Modal Biometrics (MMB) system was given by most researchers for increasing identification performance and providing more security[27].

The inherent problems of user inconvenience along with system inefficiency are solved by the MMB systems[28]. MMB systems can manage the issues of non-universality and can limit imposters from spoofing biometric attributes of authentic people. Thus, it could full fill challenges [29]. Sometimes, the usage of disparate identities of the same trait rather than utilizing the details of disparate modalities is an MMB. For example, finger

shape along with vein, fingerprints as well as finger knuckle point print of an individual human finger are the amalgamation of different traits, which are employed in multimodal finger authentication [30]. A biometric system centered upon the biometric attributes of the traits. The unique features are utilized for comparison along with matching, which is sorted out as of the biometric data (raw) [31]. For improving performance, the features from different traits are merged together. Therefore, the main method involved in MMB is fusion [32]. A combination of disparate features of traits is the definition of multiple modal fusions [33]. This biometric system's accuracy is considerably affected by the scheme of fusion, which is effective.

2.2 Fusion Schemes in MMB

Feature-level, sensor-level, Rank-Level Fusions (RLF), matching Score Level Fusions (SLF), along with decision-level fusions, are the five modules in the MMB system through its fusion [34], [35]. Different classifiers and predictors with the estimators are utilized for fusing the information largely after fusion and are composed of '3' types, namely fusion before matching, fusion at the time of matching along with fusion after matching called, pre-mapping, midst mapping, along with post mapping respectively [36].

2.3 Extrinsic & Intrinsic Biometric recognition Approaches

BR approaches can be classified into two, one is based on extrinsic biometric traits and other is based on intrinsic biometric traits. Extrinsic traits are like iris, palm print, fingerprint, face, and intrinsic traits are like palm vein, dorsal hand vein, and FV.

Extrinsic Biometrics is more vulnerable to faked input, which results in security problems. Since intrinsic modalities are hidden beneath the skin, they are hard to be faked, therefore, safer [37], [38].

Face recognition, fingerprint recognition, along palm print recognition are several BR techniques utilized recently. But, the methods were most susceptible to faked input, spoof attacks, external damages, and impersonation, which produced security issues [39], [40].

For resolving such issues, FVR technology is broadly utilized for human verification. Therefore, owing to its unique identification along with proper authentication, the FVR technology is a suitable Biometric Recognition method [41][7].

2.4 Finger Vein Biometric Recognition system

The minute blood vessels inside our fingers that are distinctive to each individual are FV[42]. The blood vessels with hemoglobin are recognizable as a sequence of dark lines while passing infrared images [43]. Only from a living body FV images could be captured; therefore, if the person is dead, it is impossible to steal the identity. Furthermore, FVR is not influenced by the weather, the age, and it is beneath the skin. It is comparatively secure and more steady [44].

Image acquisition (IA), feature extraction (FE), pre-processing, along with matching are the disparate stages for recognizing the FV images in CAD [45]. An Infrared LED light is transmitted via the finger together with attains a higher contrast image in the IA phase[46]. By conducting a few operations, like resizing, scaling, and CE, the information (unnecessary) in the image (input) is eliminated in a pre-processing stage. The major stage in FVR is the FE. Here, as of the image (pre-processed), the most informative features are extracted. For recognizing individuals, it is basically utilized [47]. The final step is matching; here, to check whether the image (input) is authentic or not, the input's likeness and the enrolled templates are contrasted[48]. But, the FVR was more precise along with it possessed a lower FRR along with False Acceptance Rate. It also presents a few drawbacks concerning extracting the FV patterns from low contrast finger images. It also possesses an

image classification issue[49].

For conquering such challenges, Zone-centered Minutia Matching[50], Support Vector Machine and also neural network (NN) method [51], Convolutional NN (CNN) [52], Lightweight CNN (L-CNN) [53], and also Deep learning (DL) methods are the several methods that are presented. Because of poor image restoration, information loss during FE, and reduction, the classification Accuracy (CA) was not efficiently addressed by the scheme, although the prevailing methods possess a higher degree of privacy and higher recognition rate (RR). It also exhibits different problems like a deficit of training data's availability, uncertain image portrayal, misalignment, restricted CE, need for high storage space for large templates along with noise amplification [54].

Wenhao You et al. [55] presented a bilayer restoration technique that dealt with skin scattering along with enhancing the FV image's visibility. The inherent factors were also examined that caused the FV image's degradation. Hence, the scheme enhanced the blurred image's clarity, enhanced the venous network, and was more dependable in FV image restoration. Concerning robustness and restoration performance, the method had surpassed the other techniques, as shown by the investigational outcomes. However, it possessed a noisy data drawback.

CihuiXie et al. [56] presented a method intended for the FV authentication centered on CNN and also supervised discrete hashing (SDH). The SDH's inclusion as a CNN had attained the most precise performance, which utilized the triplet-centered loss function. Superior outcomes over other deemed CNN architecture were attained by means of the proposed work and also proffered a considerably decreased template size. However, low accuracy rates were shown by the scheme.

Tong Liu et al.[57] introduced a Direction-Variance-Boundary Constraint Search model

and reinstated the broken FV patterns. Broken branches of FV patterns were not only effectively restored by the scheme but also enhanced the FVR performance drastically. The scheme decreased the FVR error rate from 0.57% to 0.29%, as exhibited by the investigational outcome, but it had a drawback of time consumption.

Ismail Boucherit et al. [58] formed an enhanced deep network called Merge CNN that utilized numerous CNN with shorter paths. The augmented RR with more precise identification was the method's major aim. The scheme competed with top-notch methods with a 99.56% RR, as shown by the experimentation outcome. However, it had a drawback of lower image quality.

Weili Yang et al. [59] developed a lightweight CNN named the FVR and Anti Spoofing Network (FVRAS-Net), which incorporated the recognition task together with the anti-spoofing task on a merged CNN by the Multi-Task Learning approach's usage. The more instructive image for FV identification was automatically chosen by the scheme, which efficiently enhanced the recognition performance. Furthermore, greater security along with strong real-time performance was attained by the scheme. Therefore, outstanding performance in recognition and also anti-spoofing tasks was attained by the technique as illustrated by the experiments. But, there prevailed a data scaling drawback.

Tao Zhan et al. [60]created a scheme centered on FV patterns, which utilized block uniform local binary patterns along with block 2 directional 2 dimensions principal component analysis technique. Thus, the data redundancy was efficiently decreased by the scheme, along it was more feasible. A RR over 99% was attained by the scheme, as shown by the investigational findings; however, the system needed higher computational power.

Vein-based Recognition has been one of the most popular research areas relating to biometric Recognition[61]. Today, it has many challenges ranging from designing

appropriate sensors, external environmental factors such as temperature, humidity, misplacement or misalignment of the finger, physiological changes, occlusions, illumination variance, shading, and many more. Still, it also has many inherent advantages, such as it cannot be forged; only a living person's vein pattern can be extracted, which enhances its security. Its capturing environment is amiable.

The typical steps in a person's identification using finger veins are shown in figure 2.1 [61].

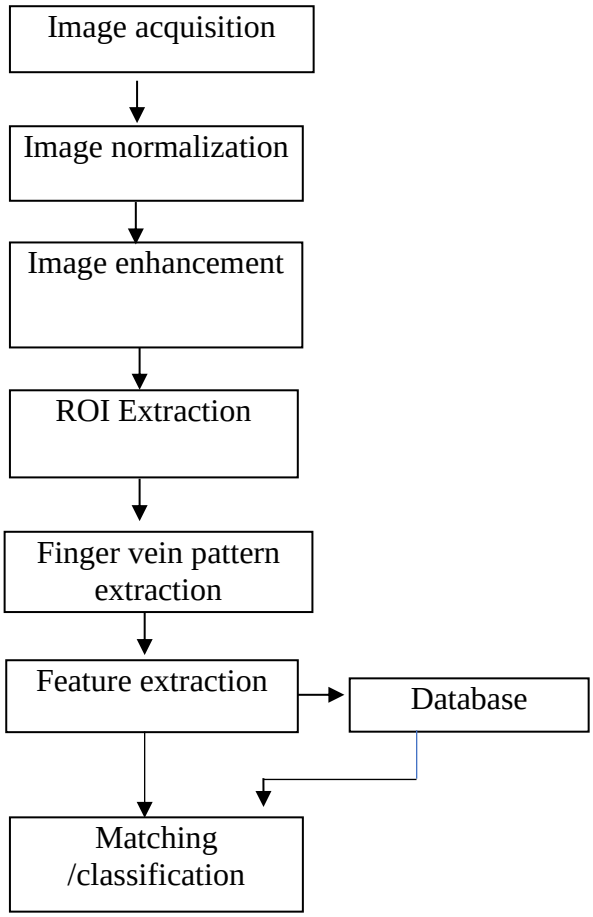

Figure 2.1:Shows typical steps generally followed in a finger vein recognition.

Person recognition using finger veins can be grouped into different categories, namely-

2.41 Whole finger vein pattern-based, also referred to as non-vein region-based.

2.42 Finger vein pattern-based- A vein point is identified using these techniques by detecting an association between the present location and its surroundings pixels –These

methods can be categorized further into – point pattern-based (including both finger vein region and non- vein region

In [62]author has used distance and spatial distribution to improve recognition accuracy. The Author uses two-step processes. In the first step k-nearest neighbors method, the initial probe is taken using the nearest centroid neighbors. The nearest centroid is scattered over the investigation and as close to the probe as possible.

In the next step, the probe is grouped using the sparse representation technique on selected k-nearest centroid neighbors. The Author reported an improvement in terms of recognition accuracy and processing time. These results are obtained as the training sample space for SRC-based grouping is minimized by using the nearest centroid neighbors,

However, the Author uses some manual cropping for the HKPU finger vein database. Manual cropping can be replaced with some automated software algorithm.

In [63], the author proposes how to generate a template with the least intraclass variation (distance). The author proposes the weighted LSR (least Square Regression) based model. This model will not only generate but also improve the template to be enrolled. This process of the generation of a template is converted into an optimization problem. Once the template is generated, an improvement model is used to improve the template vein features. Authors claim that it's the first kind of work

The author merges the multiple templates of the same class to create a template which is termed a super template. This super template is updated with the vein features from the set of vein images that are acquired during the verification of users. The main idea behind the improvement of the vein template is that the vein pattern changes slightly when it is captured at different intervals of time.

In[64]the author proposes that finger tissue intensity distribution can be used along with core biometric and termed it soft biometric. The finger image is usually separated into two foreground & background layers. The foreground layer holds texture details. The other layer holds intensity details, and these details are used as a secondary trait for identification.

The author uses two different algorithms for separating foreground and background layers. One is the existing image layer separation algorithm based on relative smoothness as in [65] while the other is the Gaussian blur. The author also states that Gaussian blur is more efficient in terms of layer separation, noise suppression, and computing time and also highlights intensity distribution in the background layer.

2.43 Soft Biometrics

The author extracted various soft features and found that an array of means & variance give the best performance when combined with the texture as the primary trait of finger vein. Here the question arises can we use vein structures as a primary trait rather than using texture

The author also proposes a rotational correction by a gradient map. The authors also mention the following soft biometric traits that are already reported –

finger shape,

width of phalangeal joint

a. distance between finger edge and image centroid.

In[66]For identification objectives, the researchers use both veins as well as non-vein points in the finger vein image. Here Author categorized image points into 2 groups, the first group is vein points (VP), and the 2nd group consists of points other than the vein, termed non-vein points (NVP). These VP or NVPs are arranged in the order of their feature

value in their respective groups. The grouping threshold is calculated and is used to make groups of NP or NVP

Matching between the test image and the database is done by classifying the points both (VP and NVP) of the test image. Then with the help of point location and point orientation, these points are arranged as matched points and non-matched points with the database.

Authors use this point grouping method in two existing vein-based recognition methods. One vein extraction uses the anatomical structure (ASAVE) [67]and the other is a multi-orientation Gabor filter [68].

Points that are overlapping are used to calculate the similarity score, and non-overlapping points are used for the dissimilarity score. How to use this method of point grouping in other approaches that uses image points can be explored.

The feature values can be used to extract venous and non-venous points and group all the image points in a vein-point approach. However, the grouping of points via attribute values by all image point approaches like LBP, etc., still needs more analysis.

In [69]for enhancing venous images, the authors use the Pulse Coupled Neural Network (PCNN). The improved images of the finger vein maximize the accuracy of identification.

This PCNN model has reduced computational complexity and higher efficiency. Further, the model parameters are calculated automatically without any training or empirical setting. One can also explore whether this model can be used for finger-vein image segmentation?

In [70]uthors proposed finger multimodal biometrics and used the graph-based method to extract features from three different modalities of a person, which are fingerprint, finger vein & finger knuckle print. The author also proposed an imaging system that captures

these three modalities. The author uses a model for graph structure with weights that extract features.

The basic assumption over the graph is that the local region has a high correlation with adjacent or surrounding regions than the far distant regions.

The graph is written like G (V, E, W), in which they have labeled V: Virtex, E: edge, and W: weight associated with the edge. For developing the graph, the image is divided into small blocks. These blocks are used in feature extraction. These features are represented as vertices in the graph. Once the features are extracted, a feature-level fusion is performed.

The authors use two types of fusion – one is serial fusion in this fusion weighted graph of each modality which can be represented as the compressed sparse row combined from the overall feature vector. Then classification algorithms such as SVM, Extreme Learning Machine (ELM) & Softmax classifier are chosen, and their performance is compared.

The other fusion method is coding fusion which combines the earlier generated three feature matrices (also called Adjacency matrices) by using competitive coding. Then either a classifier or a matrix matching algorithm can be applied for recognition purposes. Obtaining graphical features of the finger trimodal images addresses the issue of scale discrepancy, which is crucial for efficient and robust fusion. Further scope for the improvement in Graph feature accuracy by using an image repainting model is left for future work.

Graph Convolutional Neural networks (GCNNs) have better outcomes in processing graph structure data; As a result, the Author uses GCNNs to recognize finger trimodal images based on graph features.

For further work, a deep fusion model for finger tri-modalities based on GCNNs is to be developed.

In [71]authors proposed a pose correction method for reducing the finger pose variation in finger trimodal images.

The authors also proposed a method for reducing the effects of illumination variation on the finger images. The pose angle can be measured using the finger's edge line

, and hence it is corrected by rotation of the finger image. The image finger is rotated about the center of the finger direction line.

After the pose is corrected, the side background is eliminated using the ROI extraction technique. Three different ROI extraction techniques were used for three different modalities, namely – the core detection method for fingerprint [72], convex direction coding method for Finger Knuckle Point [73], and interphalangeal joint prior procedure applied on finger vein image [74].

Once the ROI is extracted, the image is enhanced using k-channel, even symmetric oriented Gabor filters. The filtered image contains local positions and gradient features. A Gabor generalized method with symmetric local graph structure (G-SLGS) [71]is proposed that considers the relationship of the target pixel with its flexible surrounding. Finally, these GSLGS are coded. Coding is done in two steps 1.-The center pixel, and its neighborhood pixels are compared in succession; if the value is greater than 1, it is assigned binary 1; otherwise, 0. Step2.- Maximum value of all the coded values is selected as the value of the target pixel.

A block-level gray histogram is plotted for each of the modalities. These block-level histograms for each modality are fused separately in series. Finally, all the three gray-level histograms are fused to generate one histogram for each of the finger tri-modal images. These histograms can be classified using SVM, ELM, and k-NN. The author uses a similarity score for matching the two histogram features. The similarity score is calculated

based on the intersection of the two feature vectors. The author indicated that the dimensionality of the feature vector could be reduced, the proposed local coding algorithm can be applied to other biometric modalities, and other fusion techniques can also be explored.

In [75]authors use multimodal biometric finger vein and palm vein and use score level fusion. Fusion is completed using fuzzy logic. In this article, Enahancement of the palm vein image is performed using CLAHE, while the enhancement of the image containing finger vein pattern is performed by adaptive histogram equalization(AHE); CLAHE is generally applied to have overall improvement of contrast.

For feature extraction, a modified 2-D Gabor filter is applied in hand vein images. Gabor filters are unaffected by changes in light, rotation, translation, and scale.

A smoothness parameter η is introduced in the Gabor filter definition. The extraction of features from palm veins is done using a gradient-based feature detection method.

Firstly the gradient magnitude and gradient orientation are calculated at each pixel level. If both exceed the threshold, then it is considered a part of the feature vector.

For matching, individual finger and palm images are compared using the Euclidean distance metric. This metric is then passed as input to the fuzzifier. The fuzzifier converts it into a matching score –as low, medium, and high. If the matching score from the fuzzifier is high for both modalities, then only a person is said to be recognized.

Future work consists of combining the attributes of the finger and palm veins at various levels, such as the feature level[21] stage. Another level could be at the decision level, and then analyzing the results, the proposed work may be extended. Other distance measurements, such as city block and Hamming distance, and Hausdorff, can also be used to compare vein features.

In [76]hese authors define a local learning method that preserves manifold structures of pixel difference value (PDV). Specifically, an asymmetric graph is constructed in such a way so that every point is made up of Its K-nearest neighbor anchors that are combined in a linear way. Finally, using unsupervised learning techniques, a feature map is obtained that maps these PDV into binary codes. These binary codes are of low dimensionality. Here Author also combines the two existing methods, Discriminative Binary Descriptor and Anchor Based Manifold Binary Pattern (AMBP) [76] at the feature level (image representation level) that improves the recognition accuracy. In this paper, future work will be on the application of this algorithm to other biometrics like palm vein-based recognition.

In [77] this Author proposes a bilayer restoration method that tries to sort out skin scattering in finger images, including dorsal images, thus enhancing the overall images that have vein patterns but it has noisy data background.

In [78]Author uses two-finger vein images, which they call composite images, and uses them for authentication. A 3-channel composite image is formed. This composite image is used on the input side of CNN. Authors claim that this method does not make the difference image as the input, therefore less prone to noise. Also, this method uses all the layers of CNN, which improves accuracy. The authors use a deep, densely connected convolution network, which is termed as DenseNet. One of the reasons that CNN is used in Recognition is that the preprocessing technique does not affect the CNN results. The author also uses a shift matching technique to overcome the effects of misalignment of finger vein images during enrollment and test probe images.

Here authors use the whole finger image after extracting from ROI as the input for the CNN. Also, they use the practical scenario, i.e., classes used in training are different from

testing or probe image. However, the authors do not use the thick part (leftmost) and the nail part (rightmost) of the finger vein image owing to poor lighting

The author also does not use the bright light areas of the image as obtaining a vein pattern in that area is difficult.

Further, it is possible to increase processing speed while maintaining accuracy. DenseNet can be made more efficient By minimizing the number of layers and transition layers. Also other modalities related to veins may be analyzed from shift matching.

In [79] author uses block uniform LBP and block 2-directional, 2-D PCA method for vein pattern recognition. In this method, author is able to reduce the data redundancy with improved performance. Table 2.1 shows Existing Different approaches for Non-Vein pattern-based methods.

Table 2.1: Existing Different approaches (That uses the whole finger, also referred to as Non-Vein pattern-based methods)

LBP Based	**Minutiae & Key points of SIFT based**	**PCA based**	**High-level features based**
Poor discrimination ability Low recognition rate	Finger vein images have a small number of minutiae. Low recognition rate	In these methods, a larger number of images are used to obtain a transformation matrix through training, and this is normally not possible	the recognition process is time-consuming It gives a high recognition rate with less consistency

		in real-world applications.	
Various Local feature extraction methods are:- LBP LLBP ELBP DBC BMULBP Global Feature extraction methods PCA Super pixel-based feature(Superpixel histogram	finger displacement and vein deformation are major issues		

In the Vein pattern-based methods approach by through observing the interaction between the present point and its neighboring points, these methods were able to locate the vein point. The selection of the nearby points in the vein point identification will be used to classify these approaches. It is listed in table 2.2.

In [80] author proposes a method that tries to overcome the effects of breaks in the vein pattern. A Direction-Variance-Boundary Constraint Search model is used for restoring gaps in vein patterns drawback of this method is that it consumes a lot of time.

Using the intrinsic finger vein recognition performance is not satisfactory because of defective vein network extraction and weak matching. A thorough examination and analysis of the vein's anatomical structure are required.

Table 2.2: Vein pattern-based methods approaches

Cross-sectional profile	**based on Neighborhood area: -**	**based on full image: -**
The vein of the cross-sectional profile is typically less grey than the others. The profile can be represented as a valley in shape. earlier approaches	Wide line detectors (WLD) along with Gabor are used to characterize the current point; the neighborhood has a predefined radius. If the number of neighbors with higher pixel values exceeds the predefined threshold, the current pixel is a vein point.	The valley-like vein pattern was observed using this approach, which represented the finger vein image as a 3-D geometrical structure and used the negative mean curvature to detect it.

1. repeated line tracking The depth of the valley is used to trace the vein point after it has been found .Finally, vein pattern is labeled by the tracking times(in binary). **2. region growth** In vein point identification, the grey value is used to consider the valley's symmetry. **3. maximum curvature point** To find the vein pattern's center line, the cross-sectional profile's local maximum curvature is determined. This process is carried out in four different directions.	One of the papers constructs a series of self-similar Gabor templates. These templates are used to obtain the vein pattern by performing convolution of templates with finger vein images.	

The central lines obtained are then fused by optimizing the curvature value on each pixel. **4. Wide line detector(WLD):** The grey value is taken from a circular neighborhood area in this case.		
All of these approaches use template matching to match the number of matched vein points.		

Gabor filter is generally used in various biometric modalities and is generally used for obtaining texture and orientation information contained in the image as given in table 2.3.

Table 2.3: shows the various methods that uses Gabor filter.

Methods	**Biometric modalities**	**Pros/cons/works**
Gabor wavelets [81]	Palm vein features, finger Vein Features	Insensitive to rotation and shift variations, variation of intensity can be handled effectively
homomorphism [82] filter and a Gabor filter	Finger Vein	It increases both the illumination and the reflectance of an image at the same time; therefore homomorphic filter is applied to enhance image contrast.
Gabor filtering[83]	Finger Vein	Image enhancement is performed, and thus the issue with the low contrast vein image is rectified with this algorithm.

		The author has solved the issue normally associated with histogram(HE) equalization that is losing the details of HE algorithm,

Methods that apply CNN / Deep Neural network in Recognition using finger vein pattern are shown in table 2.4

Table 2.4: Various methods for FV pattern extraction that uses CNN/ DNN.

Methods	**Pros/cons/applications**
Radon Transform is used for extracting features while The artificial neural network is used for classification [84]	Used in driver recognition. Radon transform is used to capture information available in limited high-valued coefficients
To isolate features, a CNN with four layers is used, and Euclidean distance is used to find the nearest match. [85]	Advantage - simultaneously extraction of features is possible, It reduces data dimensionality, and classification is performed using one network structure. It is also robust to noise and small misalignment
light convolutional neural networks [86]	It uses the center loss function. Also employs dynamic regularization in CNN

Lightweight CNN [87]	Addresses Variations in finger thickness and vein pattern induced by finger axial rotation that degrades image quality. However, accuracy needs further improvement
Merged CNN[88]	Uses many similar CNN with shorter paths. Similar CNN is inputted with different quality images. However, lower-quality images affect the accuracy
Two-stream convolutional neural networks[89]	It has a 2-channel network that has only 3 convolution layers. Focuses on displacement problem. Mini ROI is identified and finally merged with the original image, which yields better results
CNN with Supervised Discrete Hashing[90]	It enhances performance also it reduces the template size requirement, but still, accuracy remains the foremost issue, and it requires a two-step training phase
Uses CNN & recurrent neural network (RNN)[91]	Constraint-free finger vein recognition. Uses an array of cameras to capture images. Image restoration is used. RNN is used to handle multiple frames. a long Short term memory (LSTM) network is used to process Hand movement in image frames. Exposure time affects recognition accuracy

In this [92] author has discussed various loss functions that are used in the CNN and how these loss functions improve recognition accuracy by improving the variation between

inter-class subjects and decreasing in case of intraclass. This has been explored on the hand, palm, and finger vein modalities. The author also emphasizes that if we initialize CNN with the weights that have been obtained by training, using a large dataset will improve accuracy.

2.5 Review of Various Techniques

Brief Review of various basic techniques, based on which other techniques are used in this research work.

2.51 Plateau Histogram Equalization (PHE):

One of the objectives of image enhancement is to bring out the details available in the image which are not visible due to poor brightness or contrast.

Histogram Equalization (HE) is one of the most commonly used enhancement techniques for contrast enhancement of digital images. This technique defines the intensity transformation by using the properties of the image. It changes the average or the mean brightness of the image[94], [95]. A drawback of this technique is that it produces saturation effects as it tends to stretch the intensity level to extremes.

This drawback is overcome in the Plateau Histogram Equalization (PHE) technique. This PHE technique does not change the brightness and improves the contrast of the image in a controlled way, and also restricts the amplification of the noise. In this technique, the enhancement rate can be written as in equation (2.1)

$$\frac{d\,c(x)}{dx} = \mathrm{p(x)} \qquad (2.1)$$

Where c(x) is the cumulative distribution function and p(x) is the probability density function. A plateau threshold or clip limit is chosen that clipped the histogram, and the clipped histogram is redistributed in the histogram bins.

The PHE of an image $I_{th}(x)$ can be written as shown in equation (2.2)

$$I_{th}(x) = \begin{cases} I(x) \; for \; I(x) \ll Th \\ T \;\; for \; I(x) < Th \end{cases} \quad (2.2)$$

For an 8-bit image, x varies from 0 to 255. The cumulative distribution histogram of the image $H_{th}(x)$ can be written as shown in equation (2.3)

$$H_{th}(x) = \sum_{i=0}^{x} I_{th}(i) \; for \;\; 0 \ll x \ll 255 \quad (2.3)$$

$$PHE\ (x) = \left\lfloor \frac{255.H_{th}(X)}{H_{th}(255)} \right\rfloor \quad (2.4)$$

Equation (2.4) is the enhanced output image. If threshold Th = $I_{max}(x)$, then it is simply the histogram equalization. The major issue in this PHE technique is how to calculate the threshold value automatically.

2.52 Contrast Limited Adaptive Histogram Equalization (CLAHE):

Initially developed for enhancing the medical images[96]. This method divides the image into contextual regions. Then the histogram of the contextual region is analyzed. Then the center image pixel intensity is replaced by the rank of that intensity in that particular histogram. After performing this operation over the whole image, the output image is the enhanced image. The contrast enhancement at each intensity level is limited by the maximum value (clipped value) configurable by the user. Finally, the clipped pixels are redistributed uniformly.

2.53 Watershed Segmentation (WS) algorithm:

This WS algorithm is initially used in segmenting the medical images. This is used in selecting the image pixels of the same range. It is also used to reduce the noise in the image. Over segmentation is one of the issues of this algorithm, along with sensitivity. WS

algorithm transforms the 2D image into 3D one, where the intensity level corresponds to the third dimension, and the maximum intensity level corresponds to the peaks while the minimum value corresponds to the valley points[97]–[99]. WS algorithm views the image as a topographic relief area where the height can be considered as the intensity of the pixel. If waterfalls on this relief, it reaches the local minimum. The WS of this relief is the limits or the boundary of the adjacent catchment areas where water can reach.

WS algorithm defines two areas one is referred to as catchment basin, and the other is referred to as watershed lines. The catchment basin is the point where if water drops are placed, drops will reach a local minimum, and watershed lines are the points where if drops are placed, they will fall with equal probability to one of the local minima. The purpose of the WS algorithm is to find the watershed lines, which are actually the boundaries of the various regions, and hence segment the image.

In this algorithm, one can view as holes are punched in the local minima. Water is allowed to rise from these holes. As the water rises, it is not allowed to mix with the water from the adjacent areas. Further, to prevent the mixing of the water, dams are built around that area. This rise of water or flooding continues. It reaches a point where only the dams are visible when looked at from the top. These dams are the WS lines or boundaries which segment the image.

2.54 Kernelized Linear Discriminants Analysis (KLDA) algorithm:

The LDA can be generalized with kernel function to work as a non-linear classification process that is known as KLDA. Normally LDA is used in linearly separable data by finding the optimal projection[100] that maintains the cluster structure[101], [102]. KLDA can be used in non-linear separable data. The optimal solution in KLDA can be obtained by

solving the eigenvalue problem. It can be used in application that requires dimensionality reduction or classification.

LDA projects the data in such a way that the ratio between the group scatters and within the group scatter is maximized. That is, LDA consists of eigenvalue decomposition, which results in canonical variates. These variates will have all the class information represented in p-1 dimensions, where p is the different classes in the dataset. These variates can be arranged in decreasing order of the eigenvalue. The first few variates can be selected that have most of the information.

This allows low dimensionality representation of the original dataset.

Kernel trick: it is used to apply LDA in a non-linear fashion. This is done by applying LDA in the feature space rather than the observation space. A kernel is a non-linear map that maps the input samples to feature space, which is of higher dimensionality. Therefore, a computation-intensive to mitigate this kernel trick is applied. In kernel trick in which, the inner product of the mapped feature vector can be obtained from the inner product of the input samples, which are mapped to the feature vector or space.

2.55 Deep Learning Neural Network:

Deep learning is the basis of Artificial intelligence. A neural network (NN) is a type of cyclic network, which is a combination of a storage system and a binary system. Based on the activation function, there are two types of NN- one is discrete, and the other is continuous[103]. However, initially, there is a problem of vanishing gradient in the NN network.

The basic entity of NN is the neuron that receives data, performs some manipulation or computation, and generates the output. Further, these inputs and outputs of neurons are associated with weights. NN has different layers. Each layer consists of several neurons. Usually, it has one input and one output layer, and in between, it has a number of hidden layers. Neurons of one layer are connected to every neuron of the next layer as shown in figure 2.2. Neurons inputs are associated with weights, and neurons are associated with biases that need to be updated. By finding proper input weights and the biases of the neurons in various layers, we can train the NN to generate the proper output. The difference between the target output and the actual output of the output layer is the error.

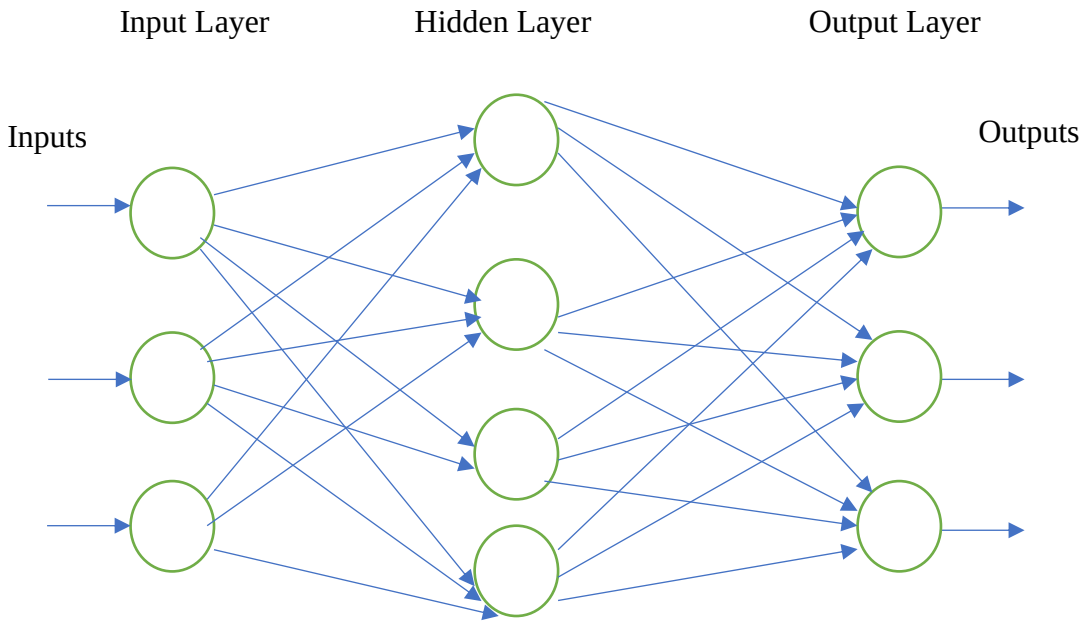

Figure 2.2: A simplified Neural network.

The backpropagation algorithm uses mean square error[104]. During the training phase, the input weights and neuron biases are recalculated many times till the target error level is reached.

2.56 Edge Detection Techniques:

Edge is one of the important features of the image, which is used in many applications, including recognition. Any abrupt change in the intensity level of the image is considered an edge. Different types of edges[105] – step edge intensity value change abruptly, i.e., from 0 to 1 or vice-versa, Roof edge- intensity changes occur over a finite distance not abruptly, and Ridge edge- where intensity changes abruptly, say from 0 to 1 and then return back to level 0. As this is a direct operation involving pixel intensity, therefore it is prone to noise. Different steps are followed to detect the edge so that it is least affected by the noise, like smoothing, enhancement, thresholding, and localization.

Edge detection techniques are classified into different categories such as Gradient-based, Laplacian operator-based, zero crossing detector, Gaussion, and colored edged detector.

Gradient-based uses 1st order partial differentiation operator while Laplacian operator uses 2nd order partial differentiation. Gradient operator is defined in Equation 2.5 below

$$\nabla f = \left[\frac{\partial f}{\partial x}, \frac{\partial f}{\partial y}\right] \tag{2.5}$$

Gradient direction and strength can be determined, which are the edge orientation and magnitude. Roberts, Sobel, Prewitt, and canny are examples. Canny has the advantage that it reduces the noise level by applying a Gaussian filter.

Laplacian operator can be written for an image I as stated below:

$$\nabla^2 I = \frac{\partial^2 I}{\partial x^2} + \frac{\partial^2 I}{\partial y^2} \tag{2.6}$$

In this, an isotropic filter is designed, which is rotationally invariant. These are less affected by the noise.

In the Zero crossing edge detection technique[106], a change in the Laplacian gradient is considered as an edge pixel. In LoG, if the 2^{nd} order derivative is zero, then it is considered an edge pixel.

Gaussian edge detector uses Gaussian filters to smooth out the noise. It is symmetrical along the edge one example is Canny edge detector.

Colour edge detector is employed for the colour images and uses 3 sub edge detectors for 3 channels and finally the edge is obtained by fusion method. It involves vector methods.

Histogram Equalisation (HE), CLAHE, and PHE are compared and shown in table 2.5

Table 2.5 : Shows the comparison of 3 contrast enhancement techniques namely HE, CLAHE, and PHE

HE	**CLAHE**	**PHE**
The average brightness of the image is changed to the middle intensity or gray level in the image	It works in the contextual region. The center pixel of the contextual region is assigned the rank depending on the intensity of the gray level in that region.	The enhancement rate is proportional to the cumulative density function (CDF). It maintains the same brightness level of the image while enhancing the contrast.

It induces saturation effects in the image as it pushes the extreme level to the highest or lowest intensity level	The contrast in the image is enhanced but limited to a maximum value that the user can select.	A threshold or the clipping parameter is used that restricts the over enhancement/ saturation issues. It requires setting the threshold levels manually

Different edge detection techniques their pros and cons are listed in table 2.6.

Table 2.6 Shows the different edge detection techniques their pros and cons

Edge Detection Technique	**Pros**	**cons**
Gradient-Based	Simple edge detectors, edge magnitude & orientation calculated	Very sensitive to noise
Zero crossing detector	Based on 2^{nd} order partial derivative. Both edge magnitude & orientation can be obtained	These are isotropic, and compared to gradient-based, these are less sensitive to noise.
Gaussian based	This gives better results even in the presence of noise.	It involves complex operations. Consumes a lot of time. Sometimes detects false edges.

LoG based	Edges can be detected at the right positions. Covers the wider area around the pixel in consideration	Does not give good results for curves and corners. The orientation of the edge can not be determined.
Color image edge detector	Results are more accurate.	Involves complex computation

2.57 Comments on the review of different techniques:

CLAHE is the enhancement technique that provides the best result for enhancing the images as it works over the contextual regions. The only concern is how to set the threshold or clipping parameter automatically rather than manually.

The PHE can invariably be used for enhancing all the input images only concern is that it is computational complex. Therefore, where output results are affected by the information contained in the image, PHE can improve the output results.

Gaussian-based edge detectors such as Canny, if used, can provide the best results in the image though it involves complex operations.

Watershed segmentation is used where precise segmentation of the image is required, though sometimes it over-segments the image, and that can be controlled. KLDA is one of the best dimensionality reduction techniques that use non-linear projection of the data or the feature vectors. Neural networks are the choice for classification where high accuracy is expected.

2.6 Research Gaps:

In the case of the MMB recognition system, the major issues remain on the robustness, accuracy, recognition rate, and how to optimize the computation cost of the recognition system. Fusion scheme to be used while choosing a combination of different biometric traits of a person.

In the case of FV biometric recognition, the major issues or challenges present are the existence of artifacts, irregular shading, distortions, etc.; precise FV detection is a difficult task that may affect the recognition accuracy. How to improve the FV pattern in FV image by processing techniques in such a way that doesn't affect recognition accuracy

2.7 Research Objectives:

To make Processing of the images of the different biometric traits efficient and effective. That can finally improve the performance of the biometric recognition system.

To propose the Fusion techniques so as to combine the different biometric traits in such a way that provides more information to the classifiers.

To propose an efficient classifier along with some dimensionality reduction so as to process the large information coming from the fusion of different biometric traits.

To propose a processing technique for the FV image with the objective of reducing the effects of illumination variations, other artifacts, and information loss during the FV enhancement stage.

To propose feature extraction technique that can extract important features from the processed image.

Selecting optimum features that are having maximum information content that reduces the feature size hence improving the overall recognition rate or accuracy and computation complexity or cost.

To full fill these research objectives the following works have been performed:

A new frame work for the MMB recognition system.

A New frame work for the finger Vein recognition system.

This chapter is based on the following work:

Ajai Kumar Gautam & Rajiv Kapoor "*A review on Finger vein based Recognition*" published in 2021 IEEE 8th Uttar Pradesh Section International Conference on Electrical, Electronics and Computer Engineering (UPCON); DOI 10.1109/UPCON52273.2021.9667572[61]

Abhishek & **Ajai Kumar Gautam** "*Study on enhancing the accuracy of fingerprint recognition system*," published in book " Recent Trends in Communication and Electronics" 2021 CRC Press, Taylor Francis Group eBook ISBN9781003193838[93].

CHAPTER 3

MULTI-MODAL BIOMETRIC RECOGNITION USING FLSL FUSION & MDLNN CLASSIFIER.

This chapter includes the details of the proposed Multi-Mode Biometric (MMB) recognition system using the Feature Level and Score Level (FLSL) fusion technique, Kernelized Linear Discriminants Analysis (KLDA), and Modified Deep Learning Neural Network (MDLNN) classifier. The Proposed methodology, results, and the comparative analysis of results.

3.1 Introduction

Today in our country itself, the three biometric traits are being used for identifying a person. The three biometric traits face, iris scan, and fingerprint scan, are stored in a card popularly known as unique identification (UID) card or AADHAR card. Govt. has decided to pass on the subsidy to the person's bank account that is linked to his/her UID card. That is a sort of multi-modal biometric recognition. Based on the biometric traits number of biometric recognition schemes exist, and each scheme has its own pros and cons; that too depends on the type of application where it is being used. However, if we combine many biometric traits along with improved algorithms, we may achieve higher performance in terms of recognition accuracy.

3.2 Proposed Method of Multimodal Biometric Recognition

This research method proposed an MMB authentication system centered on the MDLNN algorithm, which considers the face, ear, retina, fingerprint, palm print, and the geometry

of the palm together with the fingers. Initially, Improved Plateau Histogram Equalization (IPHE) enhances all the inputted images. Next, the segmentation process is executed in which the Viola-Jones Algorithm (VJA) segments the face image, and also the Penalty and Pearson correlation-based Watershed Segmentation (PPWS) algorithm eradicates the unnecessary information of the ear and finger image in addition to the blood vessels are segmented as of the retina. Additionally, the ROI calculation separates the palm region as of the front hand image.

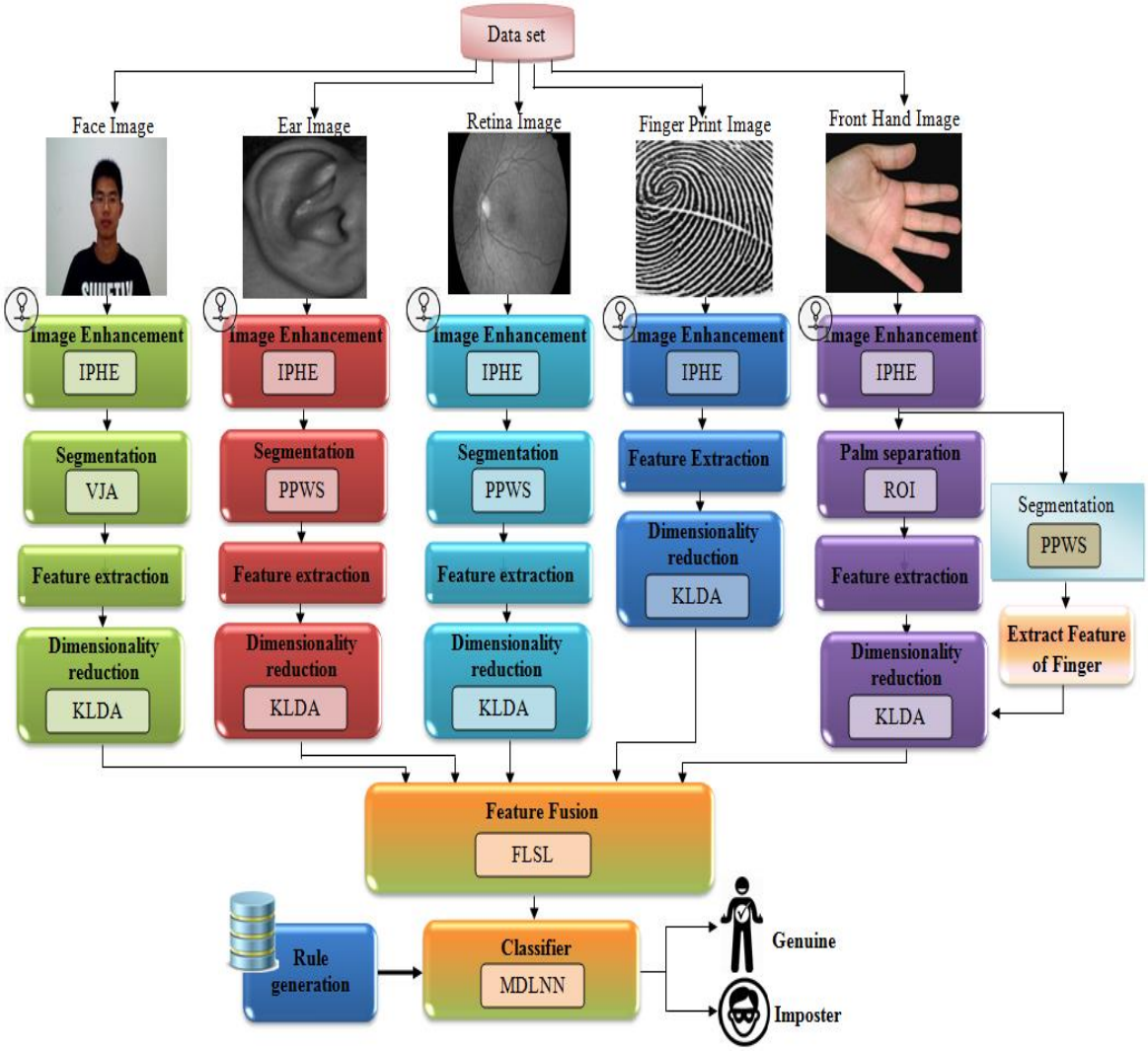

Figure 3.1: Proposed Multi-modal biometric system

As for every trait, the features are extracted. After that, the Kernelized Linear

Discriminants Analysis (KLDA) algorithm reduces the features' dimensions. After that, the FLSL fuses the features, which are then inputted to the MDLNN.

Centered on the generated rules, the person is classified as genuine or imposter by the MDLNN (explicitly, the features are trained and tested centered on that rule). Here, more hidden layers are employed in DL neural network, and the Stain Bowerbird Optimization (SBO) algorithm selects the optimal weight value for attaining higher accuracy. The proposed method's block diagram is exhibited in Figure 3.1,

3.3 Image Enhancement:

Improved Plateau Histogram Equalization (IPHE) algorithm is applied to the input images to improve the overall image contrast so that the Feature Extraction process extracts maximum information.

Over enhancement is a major issue for most contrast enhancement methods. Thus, the gamma correction function is considered here to evade that issue.

The IPHE follows these steps:

- The images' pixel values are arranged (ascending order). Next,
- The histogram building will be generated, followed by which,
- The histogram median value is calculated, which is rounded off to the nearest integer value (i.e., threshold value). After that, The EXOR operations of equivalent two histogram values are performed, and the values are considered as Cumulative Distributions Function (CDF). The image's histogram equalization is written as in Equation 3.1:

$$H_e = \frac{CDF}{A_p * N_o} \tag{3.1}$$

Wherein H_e signifies the histogram equalization, A_p implies the entire number of pixels, and N_o implies the number of output pixels.

Next, gamma correction is employed to regulate the intensity that is written as in Equation 3.2,

$$M_{i(out)} = \omega M_{i(in)}^{\chi} \tag{3.2}$$

Wherein, $M_{i(in)}$ and $M_{i(out)}$ signify the input as well as output image intensities, correspondingly, ω and χ imply two parameters that control the transformation curve's shape.

3.4 Segmentation

Segmentation of traits, say, the face, ear, retina, finger, and palm, is performed after image enhancement. Here, the VJA segments the face parts, and the PPWS algorithm is used for the ear, finger (explicitly, unnecessary information elimination), and retina. In addition, the ROI of the palm is obtained.

3.41 Face segmentation by VJA

VJA is robust, and its face detection is faster; thus, it is preferred. Here, only the face parts (left and right eye, nose, lips, as well as eyebrows) are segmented.

There are totally four sections (i) Haar Features Selection, (ii) Generating an integral image, (iii) Adaboost Training, as well as (iv) Cascading.

Haar Feature Selection: Haar features are categorized into a) two-rectangle features, which stand as the difference between the sums of the pixels among two rectangular areas, b) three-rectangle features that represent the sum of pixels among two outside rectangles and is deducted as the sum of pixels on the center rectangle and (c) four rectangle features represents the difference between the diagonal pairs of the rectangle.

Integral Image Computation: In the image, the integral image value of any point is

equivalent to the sum of the entire pixels on the upper left corner of the point. The integral image at u, v encompasses the sum of the pixels above as well as to the left of u, v, inclusive:

$$in(u,v) = \sum_{u' \le u \; v' \le v} G_i(u', v') \tag{3.3}$$

Wherein $in(u,v)$ signifies the integral image and also $G_i(u', v')$ implies the original image, $i = 1,2,.....,n,$ the face image is signified as G_1. The recursion formula is employed in the integral computation, which is described as,

$$cu(u,v) = cu(u, v-1) + G_i(u,v) \tag{3.4}$$

$$in(u,v) = in(u-1, v) + cu(u,v) \tag{3.5}$$

Wherein $cu(u,v)$ signifies the cumulative row sum, and the integral image can well be written on one pass above the image (original).

Adaboost Training: Adaboost algorithm removes redundant features and converts numerous features into a compact one. It stands as a learning classification function. Aimed at representing a face, the most meaningful ones are the chosen features. Several thousands of features can be reduced to a few hundred features by this algorithm.

Cascading: The cascaded classifier stands as a compilation of stages that encompasses a stronger classifier. Every phase verifies whether a specific sub-window is definitely not a face or maybe a face. If a specified phase classified a sub-window as a non-face, it would be discarded; whereas, if it is classified as a maybe face, it is sent to the succeeding stage on the cascade.

3.42 Palm separation

As for the improved front hand image, the palm's area is computed by computing

the ROI region. The fingers are acquired separately in this computation. Extracting ROI is a necessary task. The ROI is computed centered on the palm's rotation and also the region's size; consequently, the region's size is computed via the valleys' localization. The ROI's end result is articulated as,

$$ROI_{out} = \left(N - \frac{r_s}{2} \right) + 1 \tag{3.6}$$

Here, ROI_{out} signifies the ROI's outcome; N implies the novel rotation; r_s implies the novel region's size.

3.43 Ear, retina, and finger segmentation using PPWS

The occlusions, together with the other unwanted information (e.g., ear-rings, hair), are removed as of the improved ear image to acquire the actual ear region.

The segmentation within the ear region is handled in the ear aimed at removing the redundant information. Next, the blood vessels in the retina's image are segmented to acquire the information in the retina's image.

The segmentation procedure is implemented in the finger image aimed at the reason of eliminating unnecessary things prevalent in the image (for instance, some individual wears the rings such that the unnecessary things are eliminated). Herein, aimed at segmentation, the **PPWS technique** is utilized. The correlation calculation is executed in a typical watershed segmentation technique. However, it couldn't attain added information. Consequently, the Pearson correlation's computation is executed here; the over-segmentation issue is evaded via the penalty parameter. The morphological processes, like convolution and also Pearson's correlation, are applied in this technique aimed at locating the foreground and also background detection.

The convolution's arithmetic formulation is:

$$vol(G_i,k)=\sum_{p}\sum_{q}G_i.k(p,q) \tag{3.7}$$

Herein, vol signifies the convolution function; G_i implies the inputted image ($i=1,2,.....,n,$; the ear and retina image is signified as G_2 and G_3 ; k symbolizes the kernel. Next, Pearson's correlation is computed. The correlation is nearly alike convolution. It is enumerated as the nearby pixels' weighted summation. The correlation is equated as,

$$rel(G_i,k)=\frac{n\sum_{p,q}(u+p)(v+q)-\left(\sum_{p}(u+p)\right)\left(\sum_{q}(v+q)\right)}{\sqrt{\left[n\sum_{p}(u+p)^2-\left(\sum_{p}(u+p)\right)^2\right]\left[n\sum_{q}(v+q)^2-\left(\sum_{q}(v+q)\right)^2\right]}}k(p,q) \tag{3.8}$$

Here, (u,v) implies the inputted image's pixel location; (p,q) signifies the actual image's pixel location.

3.4 Feature Extraction

The features are extracted after the segmentation and also palm separation. For segmented face parts, segmented retina's blood vessels, fingerprint, and ear, the Local Tetra Pattern (LTrP), Gabor feature, edge, SURF, and Binary Robust Invariant Scalable Key-points (BRISK) features are extracted.

For fingerprint -The minute points and cross-line points are taken out as feature descriptors.

For palm - The geometric features, LTrP, Discrete Wavelet Transform (DWT), and SIFT are extracted

Next, the finger's geometric measurement is taken out of every finger.

LTrP: The LTrP defines the local texture's spatial structure utilizing the central grey pixel's direction. t_c Signifies the G_i image's central pixel; t_h implies t_c 's a horizontal neighbor; t_v signify t_c 's a vertical neighbor. Next, the 1st-order derivatives prevalent at the t_c is equated as,

$$G_{i\left(0^o\right)}^{(1)}\left(t_c\right)=G_i\left(t_h\right)-G_i\left(t_c\right)$$

$$G_{i\left(90^o\right)}^{(1)}\left(t_c\right)=G_i\left(t_v\right)-G_i\left(t_c\right) \tag{3.9}$$

Next, compute the pixels' magnitude $M_{G_i^1\left(t_p\right)}$ utilizing,

$$M_{G_i^1\left(t_p\right)}=\sqrt{\left(G_{i\left(0^o\right)}^{(1)}\left(t_p\right)\right)^2+\left(G_{i\left(90^o\right)}^{(1)}\left(t_p\right)\right)^2} \tag{3.10}$$

Herein, t_p signifies the image's pixels.

Gabor Feature: A '2'-dimensional Gabor function is equated as,

$$ga(u,v)=\exp\left(-\frac{u'^2+v'^2}{2\sigma^2}\right)\cos\left(2\pi\frac{u'}{\lambda}+\varphi\right) \tag{3.11}$$

$$\begin{bmatrix}u'\\v'\end{bmatrix}=\begin{bmatrix}\cos\theta & \sin\theta\\-\sin\theta & \cos\theta\end{bmatrix}\begin{bmatrix}u\\v\end{bmatrix} \tag{3.12}$$

Here, $ga(u,v)$ signifies the Gabor result; $\lambda,\theta,\varphi,\sigma,u',v'$ are the wavelet's parameters.

SURF: SURF defines a local FE technique. It utilizes a local invariant fast key-point detector to take out the image's feature key points. It utilizes a unique descriptor to take the image's feature descriptor. SURF's features are in-variant of shifting, scaling, and also rotation; it is partly invariant towards illumination and also affine transformation. Herein, the Hessian Matrix (HM) is found regarding the image G_i 's each pixel position; it is

arithmetically equated as,

$$H(u,\delta)=\begin{pmatrix} Z_{uu}(R,\delta) & Z_{uv}(R,\delta) \\ Z_{uv}(R,\delta) & Z_{vv}(R,\delta) \end{pmatrix} \tag{3.13}$$

Here, R signifies the image's point; σ is signified as scale. Generally, $Z_{uu}(R,\sigma)$ implies the convolution of the image's Gaussian 2nd-order derivative at the respective point comprising the coordinates (u,v).

BRISK: BRISK is stated as a method aimed at scale-space Key-point detection and also the binary description's creation. The Gauss function is utilized to decrement the grey-scale aliasing in the BRISK feature descriptor. The standard deviation sigma's Gauss function is proportional to the distance between the points on every concentric circle. Picking a pair as of the point pairs created by every sampling point, signified as (L_m, L_n); the grey values past the treatment are $G_i(L_m,\rho_m)$ and also $G_i(L_n,\rho_n)$. Thus, the gradient betwixt '2' sampling points $gr(L_m,L_n)$ is,

$$gr(L_m,L_n)=(L_n-L_m).\frac{G_i(L_n,\rho_n)-G_i(L_m,\rho_m)}{\|L_n-L_m\|^2} \tag{3.14}$$

Split the pixel sets into '2' sub-sets: short separation pairs (Sh) and long-distance sets (Lo). Hence, the long as well as short-distance pairs are equated as,

$$Sh=\left\{(L_m,L_n)\in A \middle| \|L_n-L_m\|<\varepsilon_{\max}\right\}\subseteq A \tag{3.15}$$

$$Lo=\left\{(L_m,L_n)\in A \middle| \|L_n-L_m\|<\varepsilon_{\min}\right\}\subseteq A \tag{3.16}$$

Here, A signifies the compilation of all sampling points' pairs; $\varepsilon_{\max}$ and $\varepsilon_{\min}$ signifies the distance thresholds. Generally, the BRISK technique is utilized aimed at solving aimed at the overall pattern's direction gr regarding the gradient betwixt '2' sampling points:

$$gr=\begin{pmatrix} gr_u \\ gr_v \end{pmatrix}=\frac{1}{Lo}.\sum gr(L_m,L_n).(L_m,L_n)\in Lo \tag{3.17}$$

Aimed at attaining scale as well as rotation invariance, the sampling pattern has been again sampled past the rotational angle $\theta = \arctan 2(gr_v, gr_u)$. The binary descriptor b_d's creation is executed by implementing equation (3.17) on all points' pairs prevalent in the set Sh via the short-range sampling points.

$$b_d = \begin{cases} 1 & G_i(L_n^\theta, \rho_n) > I(L_m^\theta, \rho_m), \\ 0 & otherwise \end{cases} \qquad \forall (L_m^\theta, L_n^\theta) \in Sh \tag{3.18}$$

Edge: Aimed at edge feature, the edge's detection techniques are employed. It comprises '5' stages: Smoothing, Finding the gradients, Non-maximal suppression, Thresholding, and then Edge tracking via hysteresis.

The smoothing stage eliminates the noise prevalent in the original image; the Gaussian filter is utilized aimed at this noise removal. After that, the sharpening alters the edge pixels detected by enumerating the image's gradient. The gradient signifies a unit vector that directs in the maximal intensity change's direction. The gradient's vertical F_u as well as horizontal F_v components are calculated initially; next, the gradient's magnitude and the direction are enumerated; this calculation is executed at the finding gradients stage. The magnitude is enumerated as,

$$\theta = \arctan\left(\frac{|F_u|}{|F_v|}\right) \tag{3.19}$$

Just the local maxima are signified as edges in the 3rd step. Next, the potential and also the actual edges are specified via thresholding; this is executed at the thresholding phase. In the end step, the edges, which aren't connected to the strong edges, are suppressed.

DWT: The image's decomposition is executed utilizing the wavelet transform. The image has been disintegrating into '2' diverse frequency bands: LH, LL, which comprise the horizontal contents and the approximate contents. The wavelet transform's definition is:

$$W_{t(di,tr)} = \int_{-\infty}^{+\infty} f(t)\,\frac{1}{\sqrt{di}}\psi * \left\{\frac{t-tr}{di}\right\} dt \tag{3.20}$$

Here, $W_{t(di,tr)}$ signifies the wavelet transform function; di, tr signifies, the dilation as well as the translation factors; $f(t)$ implies, the wavelet transformation function; ψ implies the mother wavelet's dilation.

SIFT: The SIFT technique comprises '4' steps: (a) Scale-Space Extrema's Detection, (b) Key-point Localization, (c) Orientation Assignment, and then (d) Key-point Descriptor's Generation. Scale-space functions are employed in the detection of a similar object's position as of the diverse dimensions. The scale-space function $r_g(u,v,\beta)$ is articulated as,

$$r_g(u,v,\beta) = Gau(u,v,\beta) * G_i(u,v) \tag{3.21}$$

Herein, $Gau(u,v,\beta)$ signifies the convolutional Gaussian function. The subsequent stage is the key-point localization, which is the procedure of choosing the features section aimed at locating the formerly characterized. Every key point is allotted '1' or else more orientations centered on the local image's gradient directions in the orientation assignment stage. The end process is the Key-point Descriptor's generation that targets the main key-point descriptors' creation.

Geometric Features of Palm and fingers: The palm's and fingers' geometric features are taken out utilizing the Hough Transform function. The Hough transforms detecting a line that is articulated as,

$$d = u\cos\theta + v\sin\theta \tag{3.22}$$

Here, d signifies the distance of the origin onto the nearby point on the straight line; θ

implies the angle betwixt the u axis and the line linking the origin with the nearby point. The angle's measurement is as of the line to the fingers' rotation alongside the straight direction. Next, the fingers' width is enumerated in '3' diverse positions: in the finger's top, middle, and then its bottom. The finger's 1st and end pixels are enumerated to compute the finger's width. The finger's length is partitioned into '3' segments (i.e.) top, middle, and then final; after that, the width's measurement is as of the 1st pixel to the end pixel. Next, the palm region's height and width are enumerated by building the bounding box; the palm region's area is computed by utilizing the width and also height. At last, the features taken out have been equated as,

$$B_f = a_i, \quad i = 1,2,.....,n \tag{3.23}$$

Here, B_f signifies the extracted feature's set; a_i implies the n-number of features.

3.5 Dimensionality Reduction by KLDA

As of the features taken out, necessary features are reduced by utilizing the KLDA technique. As for every trait, the features are normalized utilizing the Gaussian Kernel's function aimed at the cause of reducing the errors in the classification stage; the Gaussian Kernel's function is articulated as,

$$\ker(u,v) = \exp\left(-\frac{\|u-v\|^2}{2\xi^2}\right) \tag{3.24}$$

Here, ξ implies the variable parameter. Past the feature dimension's normalization, the class matrix's mean vector is equated as:

$$\tau_i = \frac{1}{nn_j} \sum_{dd_i \in Dm_t} dd_i \tag{3.25}$$

Here, τ_i signifies the i^{th} feature's mean; dd_i implies the i^{th} sample; nn_j symbolizes the number of samples prevalent in the j^{th} feature; Dm_t signifies the data matrix. Next, identify all the features' total mean τ. Aimed at every sample of every class, the betwixt-class scatters' matrix bc_s and also the within-class scatters' matrix wc_s is equated as:

$$bc_s = \sum_{i=1}^{n} \left(\tau_i - \tau\right) \left(\tau_i - \tau\right)^{Tr} \tag{3.26}$$

$$wc_s = \sum_{i=1}^{n} \sum_{j=1}^{n_i} \left(Y_j - \tau_i\right) \left(Y_j - \tau_i\right)^{Tr} \tag{3.27}$$

Here, n signifies the number of training samples prevalent in the class i; τ_i implies the mean vector of samples originating as of class i; Y_j signifies that class's j^{th} data. wc_s implies the features' scatter about every class's mean; bc_s signifies the features' scatter about the overall mean aimed at every class.

3.6 Feature Fusion

Next, the Feature-level Fusion (FF), together with the Score-Level (SL) fusion, is executed. Amidst all fusion techniques, this feature-level technique aids in attaining maximal accuracy in in-person identification. In FF, unwanted information can be prevalent in the features. The SL is computed aimed at reducing the information as a single quantity. FF is identified via the easy concatenation of the feature sets acquired as of the diverse traits. The concatenation procedure is equated as,

$$FF = \{a_i(G_1), a_i(G_2), a_i(G_3), a_i(G_4), a_i(G_5), a_i(G_6)\} \tag{3.28}$$

Here, $a_i(G_1), a_i(G_2), a_i(G_3), a_i(G_4), a_i(G_5), a_i(G_6)$ implies the facial, ear, retina, finger-print, fingers, and also the palm features. After that, the SL computation is centered

on score normalization; that is vital to change the various systems' scores to a general domain prior to compiling them is provided as,

$$SL = \frac{S(a_i) - \min(S(a_i))}{\max(S(a_i)) - \min(S(a_i))} \tag{3.29}$$

Here, $S(a_i)$ signifies the features' original score values. Lastly, the end feature is signified as aa_i.

3.7 Rule Generation

The rules are created to test the template image past the feature reduction. The rule generation's combination is:

i) every inputted trait is real, signifying that the person is real,

ii) every inputted trait is fake, signifying that the person is the imposter,

iii) '3' or else more than '3' inputted traits are fake, signifying that the person is the imposter, and

iv) '1' or else '2' inputted traits are fake, signifying that the individual is real.

3.8 Identification by using MDLNN

In this identification stage, the features extracted had been inputted into the MDLNN technique that finds the person regarding the rules generated. The technique comprises '3' layers. The 1st layer is the inputted layer (IL), and the final layer is the outputted layer (OL). Between the IL and OL, extra layers of units may exist, termed Hidden Layers (HLs). n- number of HLs is used in this methodology. Hence, the NN comprises the accuracy issue owing to the weight updation process such that this study technique utilizes the Satin Bowerbird Optimization (SBO) technique aimed at HL's weight value selection.

At first, the selected features' outputs are fed to the IL. The data as of the IL is inputted to the HL; in the HL, the hidden unit is enumerated aimed at the inputted features utilizing the equation (3.29):

$$hid_i = b_s + \sum_{i=1}^{n} aa_i . l_i \tag{3.30}$$

Here, b_s signifies the bias value; l_i implies the weight value; aa_i signifies the inputted features. Therefore, the HL's output is inputted to the OL. In the OL, the activation function is equated as,

$$ott_i = b_s + \sum_{i=1}^{n} hid_i . l_i \tag{3.31}$$

Here, ott_i signifies the outputted unit. Lastly, the loss function is enumerated utilizing the equation (3.31) as,

$$loss = (tar - ott_i) \tag{3.32}$$

Here, $loss$ signifies the loss function; ott_i implies the outputted unit; tar implies the network's targeted output. Past the loss computation, examine if the loss obtained matches with the particular threshold value; if it doesn't match, then the weight value is optimized utilizing the SBO technique; otherwise, the output is signified as the finalized output. Figure 3.2 exhibits the DLNN's pseudo-code

Input: Outcome of Fused features aa_t

Output: Genuine (or) Imposter

Begin

Initialize neurons, input layer, hidden layer, output layer, weight value l_t, and loss threshold ll_t.

Calculate the hidden unit and output unit by,

$$hid_t = b_s + \sum_{t=1}^{n} aa_t . l_t \text{ and } ott_t = b_s + \sum_{t=1}^{n} hid_t . l_t$$

Check loss function

if $(loss \geq ll_t)$ {

Select the weight value of neurons by SBO

// Weight updation by SBO

Generate bowers

Evaluate fitness function

while the criteria is not satisfied **do**

Calculate the probability of bowers by, $pb_i = \frac{fit_i}{\sum_{n=1}^{N} fit_n}$

if $(co_i \geq 0)$ {

Calculate fitness function by, $\frac{1}{1+co_i}$

} **else** {

Calculate fitness function by, $1+co_i$

}

end if

Change new position in each iteration

Calculate fitness function

Update elite if a bower becomes fitter than the elite

end while

} **else** {

Denote the output is the final output

}

end if

End

Figure 3.2: Pseudocode of MDLNN algorithm

3.81 The SBO technique comprises '5' stages: (a) random bowers generation, (b) probability calculation, (c) elitism, (d) position changes, and then (e) mutation.

(a) Random bowers generation: Initially, the set of bowers are created. The 1st population involves a sequence of positions aimed at bowers. Every position is determined as an n-dimensional vector of parameters. These values are initialized arbitrarily such that a uniform distribution is pondered betwixt the lower as well as upper limit parameters. The

bower's attractiveness is specified by the compilation of parameters.

***(b) Probability calculation*:** After past initialization, aimed at every population members, the probability is computed. The male, together with the female satin bowerbird, choose the bower centered on the probability calculation. The probability function is enumerated as,

$$pb_i = \frac{fit_i}{\sum_{n=1}^{N} fit_n} \tag{3.33}$$

Here, pb_i signifies the probability function; N implies the total number of bowers; fit_i signifies the fitness function that is equated as,

$$fit_i = \begin{cases} \frac{1}{1+co_i} & co_i \geq 0 \\ 1+co_i & co_i < 0 \end{cases} \tag{3.34}$$

Here, co_i signifies the cost function's value in the i^{th} position or else i^{th} bower. The cost function is the function optimized by Equation (3.34) that comprises '2' parts. The 1st part computes the final fitness in which values have been greater analogized to or equivalent to '0', whilst the 2nd part computes the fitness aimed at values lesser than '0'. This equation comprises '2' main features.

(c) Elitism: Elitism permits the finest solution (solutions) to be conserved at each phase of the optimization procedure. The position of the best bower constructed by birds is proffered as the elite of iteration. The best individual in every iteration is conserved as the elite of iteration. Elites comprise the maximal fitness values, and also it can affect other positions.

(d) Position changes: In every iteration, any bower's novel alterations can be enumerated as,

$$h_{ie}^{new} = h_{ie}^{old} + \nu_e \left(\left(\frac{h_{je} + h_{elite,e}}{2} \right) - h_{ie}^{old} \right) \tag{3.35}$$

Here, h_i signifies the i^{th} bower or else solution vector; h_{ie} implies this vector's e^{th} member; h_{ie}^{old} signifies the bower's old position; h_{ie}^{new} signifies the bower's new position; $h_{elite,e}$ implies the elite's position; h_{je} symbolizes the target solution amidst all the solutions prevalent in the present iteration; the parameter ν_e signifies the attraction power prevalent in the goal bower; it specifies the amount of step that is computed aimed at every variable. The ν_e is equated as given in equation 3.36,

$$fit_k = \frac{\nu}{1 + pb_j} \tag{3.36}$$

Here, ν implies the maximal step size; pb_j implies the probability attained by equation (3.33) utilizing the goal bower.

(e) Mutation: At every cycle's end, the random alterations are implemented with a definite probability to prevent the male from attacks, i.e., whilst the males have been busy constructing a bower upon the ground, other animals can attack them. The distribution and mutation procedure are articulated as given in equation 3.37-3.38,

$$h_{ie}^{new} \sim N_d \left(h_{ie}^{old}, \gamma^2 \right) \tag{3.37}$$

$$N_d \left(h_{ie}^{old}, \gamma^2 \right) = h_{ie}^{old} + \left(\gamma * N_d (0,1) \right) \tag{3.38}$$

Herein, N_d signifies the normal distribution; the γ implies the proportion of the space width, and it is articulated as,

$$\gamma = d(\varepsilon) * \left(h(\text{var})_{\max} - h(\text{var})_{\min} \right) \tag{3.39}$$

Herein, $h(\text{var})_{\max}$ and $h(\text{var})_{\min}$ imply the upper and lower bound allotted to variables; the

parameter $d(\varepsilon)$ implies the percentage difference betwixt the upper and lower bounds that is variable. All specified steps are continued till the fit_i is met. At last, the classifier categorized whether the person is an imposter or else real, centered on the created rule that is specified in the previous section.

3.9 Result and Discussion

The proposed multi-biometric model's performance is examined. The proposed work is applied in MATLAB. The synthetic dataset is utilized in this work for the performance analysis. The dataset's sample images, along with the further process of the image, are displayed in Figure 3.3,

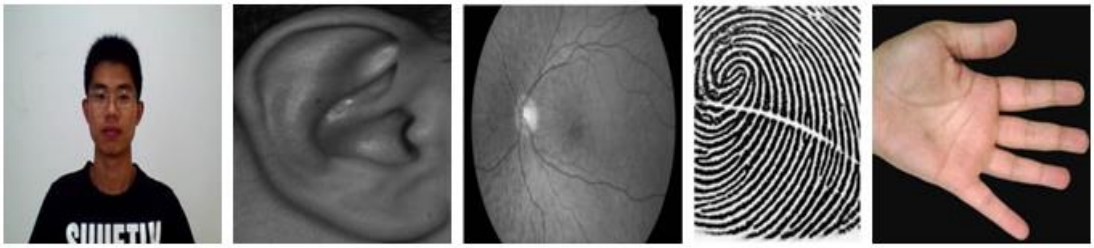

(a)

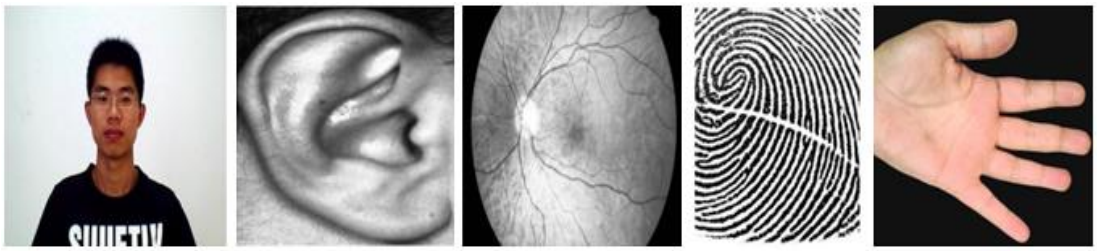

(b)

Figure 3.3: Sample images of all traits, (a) input image, and (b) enhanced image

The sample images of every trait, namely the face, ear, retina, fingerprint, along with front hand image, are demonstrated in Figure 3.3. Figure 3.3 (a) displays the dataset's input image, and the enhanced image by utilizing the IPHE algorithm is displayed in Figure 3.3 (b).

3.91 Performance analysis

The proposed MDLNN's performance is examined with the existent DL Neural Network (DLNN), Convolutional Deep Neural Networks (CDNN), along with Artificial Neural Networks (ANN) centered on sensitivity, specificity, accuracy, precision, recall, Negative Predictive Value (NPV), F-Measure, False Positives Rates (FPR), False Negative Rates (FNR), False Rejections Rate (FRR), False Discovery Rates (FDR), along with Matthews Correlations Co-efficient (MCC).

Table 3.1: Analysis of the performance of the proposed classifier with the existent classifiers based on sensitivity, specificity, and accuracy metrics

Performance Metrics	**Proposed MDLNN**	**DLNN**	**CDNN**	**ANN**
Sensitivity	0.9111	0.5887	0.2649	0.0056
Specificity	0.9555	0.7943	0.6324	0.8986
Accuracy	0.9407	0.7258	0.5099	0.6009

The MDLNN classifier's performance with the prevailing classifiers, namely DLNN, CDNN, and ANN, concerning sensitivity, specificity, along with accuracy metrics is established in Table 3.1. The ability to decide the persons rightly is sensitivity, the ability to determine the genuine persons rightly is specificity, and the accuracy metric is differentiating the imposter persons and genuine cases correctly, which is indicated as the recognition rate. Now, the MDLNN algorithm's accuracy is 0.9407, and the accuracy of the existent method is 0.7258 for DLNN, 0.5099 for CDNN, and 0.6009 for ANN. The CDNN achieves poor performance analogized to the prevailing methods along with the MDLNN centered upon the accuracy metric. Likewise, the proposed achieved a higher result, i.e. (0.9111) sensitivity and (0.9555) specificity centered upon the other '2' metrics.

The prevailing algorithms attain less performance analogized to the proposed work. It is inferred that the MDLNN-centered MMB recognition system attains a better result analogized to the prevailing methods. The graphical depiction of table 3.1 is demonstrated in Figure 3.4,

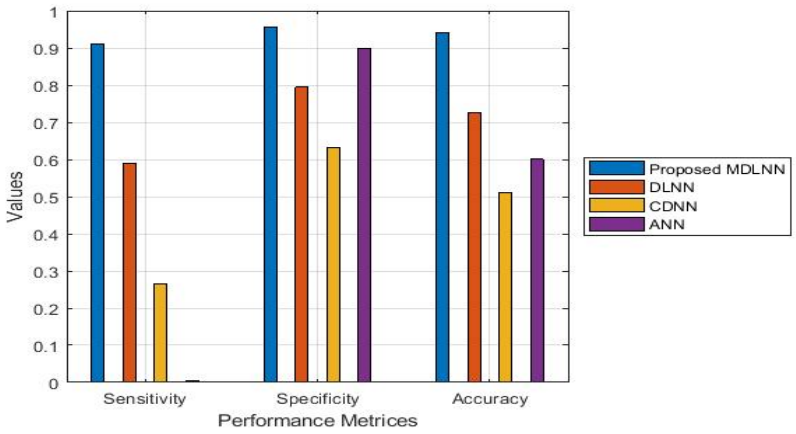

Figure 3.4: Analyses the performance of the proposed method with the existing methods based on sensitivity, specificity, and accuracy metrics

Table 3.2 demonstrated the MDLNN classifier's performance with the DLNN, CDNN, along with ANN classifiers concerning the precision, recall, along with F-Measure metrics. The number of genuine class predictions is measured by the precision metric that belonged to the genuine class; the recall measure specifies the total genuine class predictions made out of every genuine example in the dataset together with the amalgamation of both the precision along with recall metrics is the F-measure metric.

The precision, recall, and F-Measure value of the MDLNN classifier is 0.9111, and the existent methods have 0.5887 for DLNN, 0.2649 for CDNN, and the ANN has (0.0268) precision, (0.0056) recall, and (0.0092) F-Measure in this table 3.2.

Table 3.2: illustrate the performance of the MDLNN classifier with the existing classifiers based on sensitivity, specificity, and accuracy metrics

Performance Metrics	**Proposed MDLNN**	**DLNN**	**CDNN**	**ANN**
Precision	0.9111	0.5887	0.2649	0.0268
Recall	0.9111	0.5887	0.2649	0.0056
F-Measure	0.9111	0.5887	0.2649	0.0092

The existing ANN algorithm attains the worst performance analogized to the existent techniques and also the proposed methods, as concluded by this table 3.2. The existent DLNN algorithm is better than the CDNN and ANN, but it also gives lower performance than the proposed MDLNN. Therefore, it indicates that a better performance is achieved by means of the proposed MDLNN when contrasted to the prevailing research methods. The pictorial depiction of table 3.2 is exhibited in Figure 3.5,

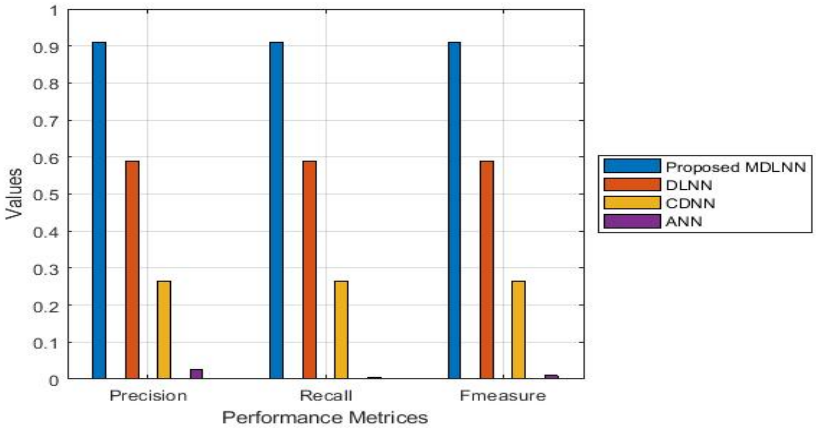

Figure 3.5: Comparative analysis of MDLNN with the other classifiers based on precision, recall, and F-Measure metrics

The performance metrics, NPV, FPR, and FNR, centered analysis are done for the MDLNN with the prevailing classifiers in Table 3.3.

Table 3.3: Performance analysis based on NPV, FPR, and FNR

Performance Metrics	**Proposed MDLNN**	**DLNN**	**CDNN**	**ANN**
NPV	0.9555	0.7943	0.6324	0.6437
FPR	0.0444	0.2056	0.3675	0.1014
FNR	0.0888	0.4113	0.7350	0.9944

Now the first place is held by the MDLNN classifiers centered on NPV metric, and hold the last place centered on FPR and FNR metrics. The last place is held by the CDNN algorithm centered upon the NPV metric. The ANN holds first place, and CDNN holds first place centered on the FPR metric. The NPV, FPR, and FNR value of the MDLNN is 0.9555, 0.0444, and 0.0888. The NPVE value of the CDNN is 0.6324. Overall, the proposed classifier has a higher NPV as of the analysis and low FPR along with the FNR result; therefore, it is summarized that higher performance is acquired by the proposed MDLNN centered MMB recognition system analogized to the other method-centered recognition. The pictorial demonstration of Table 3.3 is displayed in Figure 3.6,

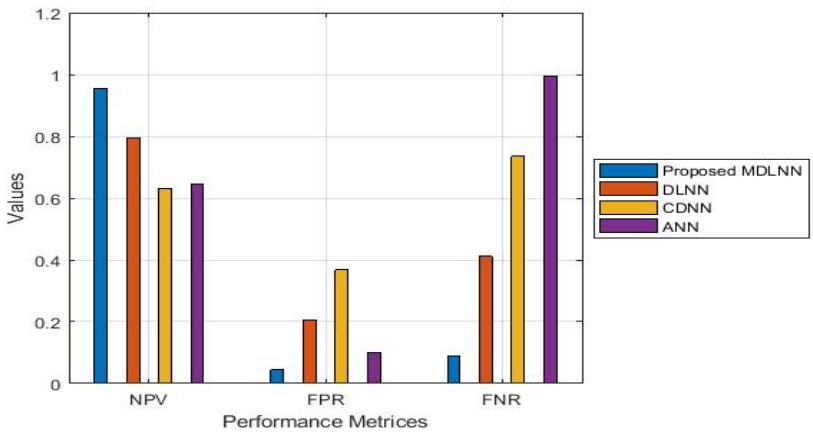

Figure 3.6: Performance analysis based on NPV, FPR, and FNR metrics

Table 3.4: Performance analysis based on MCC, FRR, and FDR

Performance Metrics	**Proposed MDLNN**	**DLNN**	**CDNN**	**ANN**
MCC	0.8667	0.3830	0.1025	0.1776
FRR	0.0888	0.4113	0.7350	0.9944
FDR	0.0888	0.4113	0.7350	0.9731

The proposed MDLNN classifier's performance with the existing DLNN, CDNN, and ANN algorithm concerning MCC, FRR, and FDR metrics is examined in table 3.4. The true classes with the predicted classes are measured by the MCC, the FRR specifies the percentage of identification instances in which authorized persons are wrongly rejected, and the total false discoveries in recognition is divided by means of the total discoveries in that recognition is FDR. Here, a higher MCC value, i.e., 0.8667, is possessed by means of the proposed MDLNN algorithm along with lower FRR and FDR values. The CDNN and ANN possess lower MCC values and higher FRR and FDR values.

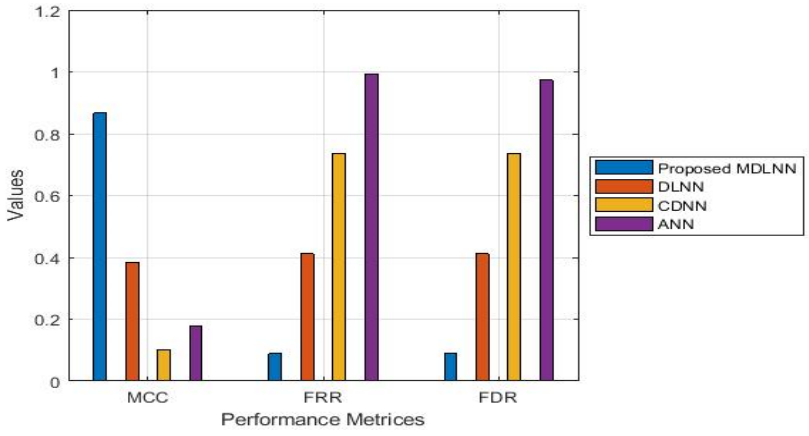

Figure 3.7: Analyses the performance based on MCC, FRR, and FDR metrics

The DLNN is much better as contrasted with the CDNN and ANN, but the DLNN also has

low performance than the MDLNN. Therefore, better results are attained by the MDLNN in multi-biometric recognition. The graphical depiction of table 3.4 is exhibited in Figure 3.7.

3.10 Significant Findings

In the Proposed MMB recognition system, input biometric traits are enhanced by the IPHE method that finally improves the Recognition Rate(RR) as more informative features can be extracted in the feature extraction stage. Segmentation is performed by PPWS algorithm that eliminate redundant information from the images of ear, finger and blood vessels of the retina. This improves the information content in the feature extraction, thus improves the overall RR.

The proposed MMB recognition system with the MDLNN classifier makes the recognition system more robust and also yields improved accuracy (also signified as the recognition rate). The proposed MDLNN accuracy is (0.9407), which is greater compared to other classifiers.

This chapter is based on the following work:

Ajai Kumar Gautam & Rajiv Kapoor "*Multi-modal biometric recognition system based on FLSL fusion method and MDLNN classifier*." Turkish Journal of Computer and Mathematics Education, ISSN: 2382-2389 in Volume 12, No. 11 (2021). [SJR-0.218] [Published in SCOPUS INDEXED JOURNAL][107]

CHAPTER 4

FINGER VEIN BASED RECOGNITION USING ES-RWCNN

This chapter includes the details of the proposed Finger Vein Recognition (FVR) system using Enhanced Sigmoid Reweighted based Convolutional Neural Network (ES-RwCNN), Trapezoid Membership Function-Based Contrast Limited Adaptive Histogram Equalization (TMF-CLAHE) details, and Local 12 direction texture pattern (L12DTP) features are explained in details. The Proposed methodology, results, and the comparative analysis of results are given.

4.1 Introduction

A new framework is proposed for identifying FV is created to offer a precise biometric authorization utilizing ES-RwCNN. The image is initially pre-processed by the framework via executing rotation, cropping, resizing, and normalization to avoid unwilling distortions. Utilizing TMF-CLAHE, For obtaining the most informative features, an Adaptive Weight Mutated Whale Optimization Algorithm (AWM-WOA) technique is proposed that enhances the model's accuracy and decreases the computational complexity (CC). Finally, to identify the authorized person, the chosen features are presented to ES-RwCNN.

4.2 Proposed Finger Vein Authentication of the user data

FV identification is impacted by performance degradation resulting from illumination variations, information loss produced during feature pattern extraction, as well as reduction and misclassification error upon image capture. To address the above issues, an ES-RwCNN is created for executing the user data's FV authentication, as exhibited in figure:

4.1

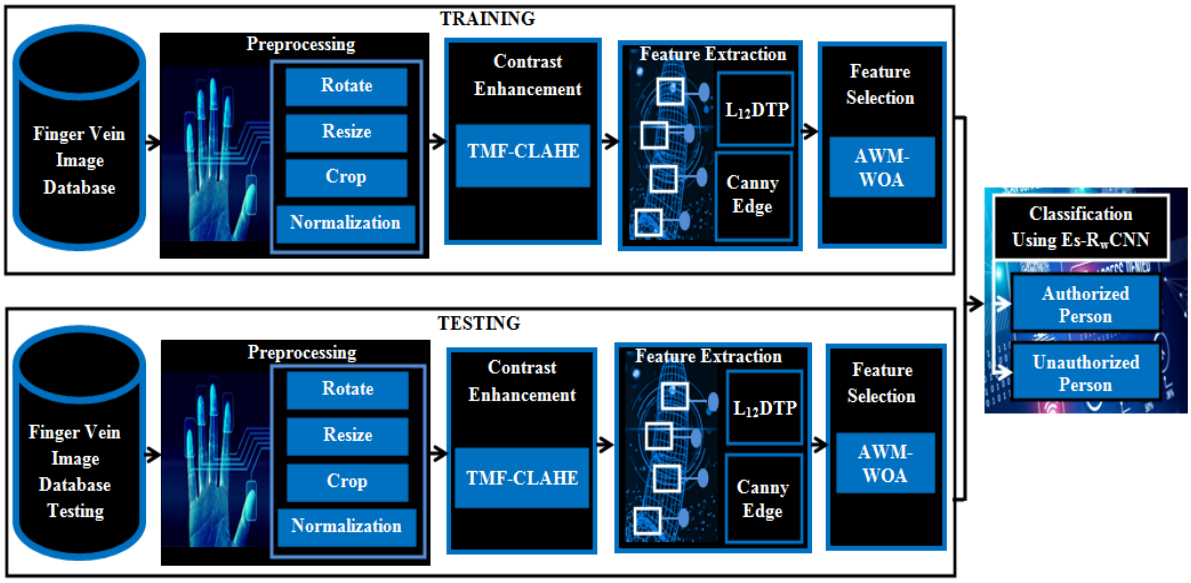

Figure 4.1: ***Finger Vein authentication system.***

4.3 Training Phase and Testing Phase

Utilizing the developed classification model, namely ES-RwCNN for recognizing the FV, various sampled images are separated into trained and tested images and processed. Disparate phases of processing, namely pre-processing, CE, FE, along with feature selection (FS), is undergone by the compilation of split-sample trained and tested images for improvising the classification outcome to identify the FV.

4.4 Pre-processing-

To reduce the unwanted distortions pre-processing of the image is performed that involves image rotation, resizing, cropping, along normalization

4.41 Contrast Enhancement

The information's perception in the image is enhanced through the CE phase. A superior result is offered by arresting the uneven shading along with vein posture deformation that degrades the FV authentication accuracy. An enhancement technique called TMF-CLAHE is created by the work. Trapezoid Membership Function (TMF) is applied by the TMF-CLAHE method for automatic determination of clipping-parameter that restricts the contrast level in an image, therefore, causing an enhanced image (EI). For attaining the EI, the proposed **TMF-CLAHE** comprises the subsequent steps:

Step1: Firstly, convert the OI intensity level into the contextual regions, which don't overlap. This region is called an image tile of dimension $\mathrm{A}\times\mathrm{B}$.

Step2: By creating the textual region's histogram in the dimensional space $\mathrm{A}\times\mathrm{B}$, the respective region is assessed.

Step3: The contextual region is gauged along with restricted with a *CL* (clipped limit) value-centered upon the histogram, such as written in eqution 5.1.

$$\mathrm{B}_{avg} = \frac{\left(\mathrm{B}_{\Gamma}x \times \mathrm{B}_{\Gamma}y\right)}{\mathrm{B}_{grey}} \tag{4.1}$$

Wherein B_{avg} indicates the pixel's average number, B_{grey} symbolizes the grey levels in the contextual region, $\mathrm{B}_{\Gamma}x$ and $\mathrm{B}_{\Gamma}y$ signifies the pixel values along the x and also y directions inside the contextual regions. Now, utilizing the TMF, the images' over enhancement along with under enhancement is lessened by establishing the predetermined clip limit, which was a primary challenge whilst fixing a pre-fixed clip limit. Therefore, the clipping parameter attained is disparate as of the image upon which TMF-CLAHE is implemented that is presented as in Equation 4.2:

$$\vartheta_{\Gamma}(\mathrm{B}_{CL}) = \begin{cases} 0 & if\left(\mathrm{B}_{CL} \le a\right)\ o\ \left(\mathrm{B}_{CL} \ge d\right) \\ (\mathrm{B}_{CL} - a)/(b-a) & if\ \mathrm{B}_{CL} \in (a,b] \\ 1 & if\ \mathrm{B}_{CL} \in (b,c] \\ (d - \mathrm{B}_{CL})/(d-c) & if\ \mathrm{B}_{CL} \in (b,d] \end{cases} \tag{4.2}$$

Wherein $\vartheta_{\Gamma}(\mathrm{B}_{CL})$ signifies the image,s clipping parameter, which is dependent, (a,b,c,d) shows the trapezoidal membership function (T_F) 's coordinates.

Hence, the clip limit is measured by the TMF, and the computed clip limit is changed on the predefined crisp clip limit. Now, the actual CL is specified as:

$$\mathbf{B}_{CL} = \mathbf{B}_{Clip} \times \mathbf{B}_{avg} \tag{4.3}$$

Here, by specific conditions, the pixel's clipping is decided; that are, the corresponding pixels get clipped if B_{CL} is lesser than a number of pixels in a specific limit of array [0, 1]. Now, that pixel's average location is decided as $\mathrm{B}_{\sum clip}$, and for every gray level, the remaining pixel's average is distributed as:

$$\mathrm{B}_{avggray} = \frac{\mathrm{B}_{\sum clip}}{\mathrm{B}_{gray}} \tag{4.4}$$

The subsequent statements in Equation 4.5 present the theory of trimming histograms:

$$\begin{aligned} &if \aleph_{region}(i) = \mathrm{B}_{CL} \\ &\aleph_{region_{clip}}(i) = \mathrm{B}_{CL} \\ &Else\, if\left(\aleph_{region}(i) + \mathrm{B}_{avggray}\right) > \mathrm{B}_{CL} \\ &\aleph_{region_{clip}}(i) = \mathrm{B}_{CL} \\ &else \aleph_{region_{clip}}(i) + \aleph_{region}(i) = \mathrm{B}_{CL} \end{aligned} \tag{4.5}$$

Whereas $\aleph_{region}(i)$ and $\aleph_{region_{clip}}(i)$ symbolizes the original grey-level histograms along with trimmed histograms of every region at i^{th} gray-level.

Step5: The remaining pixels are rearranged until every pixel has been allotted. The pixel

step's rearrangement is proffered by: $step = \mathrm{B}_{gray} / \mathrm{B}_{remain}$

B_{remain} implies the remaining number of clipped pixels. The steps are repeated till every pixel gets distributed uniformly. The vein's important selection is offered by the TMF-CLAHE CE, where the ridges are observable and distinguishable from each other, along with deeming it the ROI of the FV image.

4.5 Feature Extraction

For offering the FV's knowledge to the classification model, the features (relevant) are extracted via FE. To decrease the Computation Cost, FE assists the model along with helping with precise personal identification systems. Utilizing L_{12}DTP and also edge techniques, textural and EFs are extracted as of the EI by the proposed work. The developed extraction technique can extract both local and also global features comprising micro-patterns.

4.51 Local 12 direction texture pattern (L_{12}DTP)

Using L_{12}DTP, the texture-centered feature is extracted that separates the image into 13x13 regions. The divided region is measured along with the numerous directions, like 0°, 15°, 30°, 45°, 60°, 75°, 90°, 105°, 120°, 135°, 150°, and 165° centered upon the magnitude along with sign. Therefore, the center pixel's 12 diagonal directions in an image are formed by the pixel value. Then, by contrasting each pixel with the nearest neighboring pixel within the same direction, the 13 × 13 regions are assessed for sign operation (T_{θ_i}) as signified below

$$\begin{aligned} &\mathrm{T}_{\theta_i} = \sum_{k=0}^{k-2} \mu\left(\chi_p - \chi_{p+1}\right) 2^k k \\ &\theta_i = 0^\bullet, 15^\bullet, 30^\bullet, 45^\bullet, 60^\bullet, 75^\bullet, 90^\bullet, 105^\bullet, 120^\bullet, 135^\bullet, 150^\bullet, 165^\bullet \end{aligned} \tag{4.6}$$

$$\mu(\Gamma^*) = \begin{cases} 1, & \Gamma^* \geq 0 \\ 0, & otherwise \end{cases}$$

Wherein k symbolizes the number of neighbors and θ_i characterizes the 12 directions. Then, by analyzing the nearby absolute differences values and a global threshold, the magnitude (M_{θ_i}) is estimated. The magnitude mathematical formulation is presented below:

$$\begin{aligned} &M_{\theta_i} = \sum_{k=0}^{k-2} \mu\left(\left|\chi_p - \chi_{p+1}\right| - \alpha\right) 2^k \\ &\theta_i = 0^\bullet, 15^\bullet, 30^\bullet, 45^\bullet, 60^\bullet, 75^\bullet, 90^\bullet, 105^\bullet, 120^\bullet, 135^\bullet, 150^\bullet, 165^\bullet \end{aligned} \tag{4.7}$$

$$\alpha = \frac{1}{k-1} \sum_{k=0}^{k-2} \mu\left(\chi_p - \chi_{p+1}\right).$$

The entire image is signified by creating a histogram after calculating T_{θ_i} and M_{θ_i} as

$$hist(\mathrm{T}_{\theta_i}(l)) = \sum_{i=1}^{A} \sum_{j=1}^{B} F_2\left(\mathrm{T}_{\theta_i}(i, j), l\right) \tag{4.8}$$

$$l \in \left[0, \left(2^k - 1\right)\right]$$

$$hist(M_{\theta_i}(l)) = \sum_{i=1}^{A} \sum_{j=1}^{B} F_2\left(M_{\theta_i}(i, j), l\right) \tag{4.9}$$

$$F_2(\Gamma_i, \Gamma_j) = \begin{cases} 1 & \Gamma_i = \Gamma_j \\ 0 & otherwise \end{cases}$$

Wherein $\mathrm{A} \times \mathrm{B}$ symbolizes the input image's size and k represents the total neighbors. Lastly, the concatenation of two histograms and extraction of features is done.

$$hist_{concat} = \left[hist(\mathrm{T}_{\theta_i}(l)); hist(M_{\theta_i}(l))\right] \tag{4.10}$$

4.52 Edge detection Techniques

Different features linked to edges or boundaries are measured by Edge Detector. An extra advantage is offered by EF via enhancing the FVR detection with huge accuracy.

Firstly, to remove the unnecessary details, the image is processed in a Gaussian filter, i.e., provided as:

$$e(\Gamma_i,\Gamma_j)=E(\Gamma_i,\Gamma_j)*F(\Gamma_i,\Gamma_j) \tag{4.11}$$

$$E=\frac{1}{\sqrt{2\pi\alpha^2}}\exp\left(-\frac{\Gamma_i^2+\Gamma_j^2}{2\alpha^2}\right)$$

Then, the gradient is measured for gradient operations:

$$G(\Gamma_i,\Gamma_j)=\sqrt{\kappa_i^2(\Gamma_i,\Gamma_j)+\kappa_j^2(\Gamma_i,\Gamma_j)} \tag{4.12}$$

$$\theta(\Gamma_i,\Gamma_j)=\tan^{-1}\left[\kappa_i(\Gamma_i,\Gamma_j)/\kappa_j(\Gamma_i,\Gamma_j)\right]$$

After that, for suppressing every noisy data as of the selected edge data, a threshold value is estimated as given in equation 4.13.

$$G_T(\Gamma_i,\Gamma_j)=\begin{cases}G(\Gamma_i,\Gamma_j), & if\ \ G(\Gamma_i,\Gamma_j)>T\\ 0, & otherwise\end{cases} \tag{4.13}$$

Wherein T implies the selection in which every edge element are kept whilst numerous noise is repressed.

Next, for attaining a thin edge ridge, the chosen edge data G_T is suppressed. By checking whether each non-zero $G(\Gamma_i,\Gamma_j)$ is larger contrasted to its 2 neighbors along the gradient direction $\theta(\Gamma_i,\Gamma_j)$, each edge is assessed for thinning the edges. If so, it is kept unchanged otherwise, fix it to 0.

For obtaining 2 binary images ς_1 and ς_2, two disparate thresholds are fixed τ_1 and also τ_2 for the preceding result. There exists less noise and also fewer false borders while ς_2 is

contains a larger threshold τ_2 but has a limitation of wide edge tolerance as analogized to ς_1 with a smaller threshold τ_1.

Numerous features are calculated centered upon the edge. Therefore, a collection of features, i.e., the textural and also EF, is saved within the data frame.

4.6 Feature Selection

The most significant and informative features are extracted by the FS, which enhances the improved performance in FVR. AWM-WOA has been formed by the work for better FS. The CC is effectively mitigated by the created algorithm. Thus, the classification model's accuracy is improved with limited time and cost. The optimal solution (OS) is attained by the AWM-WOA grounded on the developed objective function that chooses the more informative feature that is offered by a sum of disparate features and forms a sole objective function formulated as in equation 4.14:

$$\xi_{objective}(\Gamma_E^*) = \xi_1(\Gamma_1^*) + \xi_2(\Gamma_2^*) + \xi_3(\Gamma_3^*) + ... + \xi_n(\Gamma_n^*) \tag{4.14}$$

Wherein $\xi_1, \xi_2, ...\xi_n$ symbolizes the constant value that provides the polarity of the features $\Gamma_1^*, \Gamma_2^*, \Gamma_3^* ..... \Gamma_n^*$.

Step 1: Firstly, the present best search agent's position is presumed as an optimum point. The other search agents update their position centered upon the best search agent centered on the optimum point. This equation is provided as equation 4.15:

$$\vec{\vartheta} = \left|\vec{k}.\overrightarrow{\Gamma_n^{\chi}}(t) - \overrightarrow{\Gamma_n^*}(t)\right|, \tag{4.15}$$

$$\overrightarrow{\Gamma_n^*}(t+1) = \overrightarrow{\Gamma_n^{\chi}}(t) - \vec{\alpha}.\vec{\vartheta},$$

Where t symbolizes the existing iteration, $\overrightarrow{\Gamma_n^{\chi}}$ implies the best solution's n^{th} position vector, $\overrightarrow{\Gamma_n^*}$ implies the n^{th} position vector of every agent along with $\overrightarrow{\Gamma_n^*}(t+1)$ symbolizes the updated position. $\vec{\alpha}$ along with's coefficients are gauged as

$$\vec{\alpha} = 2.\vec{a}.r - \vec{a} \qquad (4.16)$$

$$\vec{k} = 2r$$

Where, a is slowly reduced as of 2 to 0 and r signifies a random number at the interval [0, 1].

Step 2: The exploitation assures the searching of OS inside the limited space in this step. Further, two disparate phases are undergone by the exploitation process that is described below:

Phase 1: $\vec{\alpha}$ implies a random value within the interval $[-a, a]$ in, which a reduces as of 2 to 0 over the iterations in this phase. The new search agent position could be stated betwixt the position (original) together with the agent's updated position by setting the arbitrary values for $\vec{\alpha}$ within the interval [-1, 1]. The best OS is not attained because the updated solution gets converged over the local optimal search space. For balancing this, the whale optimization merges with the Adaptive weight factor, which is dynamically modified with an iteration number that sustains the global along with local searchability. The adaptive search scope grounded on the inertia weight function w is articulated as:

$$\begin{cases} \Lambda = w \times \vec{\vartheta} \times (rand(0,1) - 0.5) \\ w = \exp(-x_1 \times (I / I_m)^{x_2}) \end{cases} \qquad (4.17)$$

Wherein, x_1 along with x_2 in the gamut of [1, 30] are the predefined constants for modifying the search scope, present iteration, together with the maximum iteration, is indicated as I and I_m correspondingly.

Phase 2: A spiral equation is formed betwixt the whale and also prey's position that is offered as in equation 4.18- 4.19.

$$\overrightarrow{\vartheta^{t}} = \left|\overrightarrow{\Gamma_{n}^{\chi}}(t) - \vec{\Gamma}_{n}^{*}(t)\right| \tag{4.18}$$

$$\overrightarrow{\Gamma_{n}^{*}}(t+1) = \overrightarrow{\vartheta^{t}} e^{gl}.\cos(2\pi l) + \overrightarrow{\Gamma_{n}^{\chi}}(t) \tag{4.19}$$

Where the distance betwixt the whale along with prey is signified as ϑ^{t}, g implies a constant that signifies the logarithmic shape, l denotes a random value within the interval [-1, 1].

The spiral model movement is simulated throughout the algorithm's iterations that are proffered as in equation 4.20.

$$\overrightarrow{\Gamma_{n}^{*}}(t+1) = \begin{cases} \overrightarrow{\Gamma_{n}^{\chi}}(t) - \vec{\alpha}.\vec{\vartheta} & if \quad p < 0.5; \\ \vec{\vartheta} e^{gl}.\cos(2\pi l) + \overrightarrow{\Gamma_{n}^{\chi}}(t) & if \quad p \geq 0.5, \end{cases} \tag{4.20}$$

Wherein, p implies a random number in [0, 1].

Step 3: The exploration stage is conducted, which assures the searching of the OS in a broad variety of areas in step 3. The exploration stage is contrary to the exploitation stage. In step 2 $\vec{\alpha}$ is presumed as a random value that is larger analogized to 1 or smaller than -1 in an interval [-1, 1]. The search agent's position might remain distant from the whale together with its position is updated utilizing the novel mutation operator. The new offspring's diversity is enhanced by this application and assists WOA to jump out of local optima. The searching process continues from the existing solution $\overrightarrow{\Gamma_{n}^{*}}(t)$ to its nearest solution Γ_{SN} centered on the novel mutation operator given in equation 4.21.

$$\overrightarrow{\Gamma_{n}^{*}}(t) = \overrightarrow{\Gamma_{n}^{*}}(t) + \phi_{t}(\overrightarrow{\Gamma_{n}^{*}}(t) - \Gamma_{SN}) \tag{4.21}$$

Where $t \in \{1,2,3.....,SN/2\}$ signifies a random index, SN implies the populace size, and $\phi_{i,j}$ signifies a random integer $[-1,1]$.

The updated solution's position is formulated as in equation 4.22:

$$\vec{\vartheta} = \left|\vec{k}.\overrightarrow{\Gamma_n^*}(t) - \overrightarrow{\Gamma_n^*}\right| \qquad (4.22)$$

$$\overrightarrow{\Gamma_n^*}(t+1) = \overrightarrow{\Gamma_n^*}(t) - \vec{\alpha}.\vec{\vartheta}$$

Wherein Γ_n^* is an updated position vector.

In the objective solution, the attained solution is substituted; the top solution is elected as the most instructive feature. Thereafter, it is kept in a set as stated below in equation 4.23:

$$\xi(\Gamma_E^*) = \left\{\Gamma_1^* + \Gamma_2^* + \Gamma_3^* + ... + \Gamma\right\}_n^* \qquad (4.23)$$

4.7 Classification

For detecting precisely whether the finger vein is authorized or unauthorized, classification is useful. Generally, for attaining a superior classification score, the NN is mostly utilized. Whilst performing back-propagation, a vanishing gradient (VG) takes place that causes slow-down learning and also decreases the classification rate. For solving this issue, an Es-RwCNN is formed by the work for enhancing the CA for FVR.

Over the chosen features, the developed ES-RwCNN gets trained. Afterward, they are tested to compute the classification score for identifying finger veins. For obtaining training and attaining the recognition, that is if the person is authorized or not, the sample features are processed inside numerous layers. The convolution layer (CL), relu layer, pooling layer (PL), and also fully connected layer (FCL) are the layers.

1) Convolutional Layer: A set of two-dimensional convolutions betwixt the input features Γ_m^l is executed by the CL, where l and m symbolizes the levels and map indexes and the kernel filter K_m^l , i.e. provided as $\left[\Gamma_m^l\right] \times \mathrm{K}_m^l$. After filtration, the n^{th} output map λ_n^l attained by the CL is measured as given in equation 4.24.

$$\lambda_n^l = \sum_{i=0}^{n} \sum_{j=0}^{n} w_{i,j}^l \Gamma_{i,j}^l + \mathrm{B}_{i,j}^l \tag{4.24}$$

Wherein i, j indicates rows and also columns that signify the features, $w_{i,j}^l$ signifies the weight at the respective interval of l , $\mathrm{B}_{i,j}^l$ implies the bias of interval of l

2) ReLU: For studying the features, an activation function (AF) that decides which neurons must be trained or activated is Relu (act_{relu}). It supports the system's nonlinearity, and the VG issue is decreased. It enables the network's quicker training without sacrificing accuracy. The ReLU activation is proffered as given in equation 4.25:

$$f\left(\Gamma_m^l\right) = \max\left[0, \Gamma_m^l\right] \tag{4.25}$$

This layer is united with the CL and deals with augmenting the model's nonlinear properties and also the total network without influencing the receptive fields of the CL i.e.

$$\lambda_n^l = act_{relu}\left(\sum_{i=0}^{N} \sum_{j=0}^{N} w_{i,j}^l \Gamma_{i,j}^l + \mathrm{B}_{i,j}^l\right) \tag{4.26}$$

3) Pooling: An approach aimed at downsampling the feature map is presented by the PL by summarizing a feature's existence in patches of the feature map. By decreasing dimensionality, the calculation power needed for processing the data is lessened. Whilst efficiently preserving the model's training, it is employed for extracting invariant dominant rotational and positional features as given in equation 4.27 .

$$\lambda_n^p = \forall_{layers}^{+}\left(\left|\Gamma_m^l\right|\right) \tag{4.27}$$

Wherein $\forall_{layers}^{+}$ might symbolize disparate PLs, like maximum PL, minimum PL, average PL, etc. For improvising the image's quality, the PL is helpful.

A CNN's i^{th} layer is formed by the CL and the PL. For capturing the low-level information much more depending upon the image's complexity, the number of such layers could be augmented. Therefore, the output from the CL is flattened and further preceded.

$$\aleph_3^{pooling}\left(F_{Flatten}\right) = \left[\Im_1, \Im_2, \Im_3, \Im_4, \ldots . \Im_n\right] \tag{4.28}$$

4) Fully Connected Layer: An N-dimensional vector is generated, where N implies the total classes that the program has to select as of the flattened features. For categorizing the image (input) affiliated to a particular label, a Sigmoid AF (act_{σ}) is normally utilized. In FCL, the VG's drawback is possessed by the sigmoid function that generally occurred during the back-propagation method causing slow-down learning and also a reduction in classification rate. By mitigating saturation to lessen the VG issue within the network, Enhanced Sigmoid (ES) AF is designed overcome this issue. It attains superior results for classification. Let Γ_m implies the m^{th} input map of the output layer Θ_m^l. Next, the linear combination Θ_m^l is specified as in given below equations 4.29 :

$$\Theta_m^l = act_{\sigma}\left(\sum_{i=1}^{n} w_i \Im_{i,j} + \mathrm{B}_{i,j}\right)$$

$$\dot{f}_m'(\Gamma_m) = \begin{cases} \beta(\Gamma_m - a) + act_{E\sigma}(a) & \Gamma_m >= a \\ act_{E\sigma}(a) & -a < \Gamma_m < a \\ \beta(\Gamma_m + a) + act_{E\sigma}(a) & \Gamma_m \le -a \end{cases} \qquad (4.29)$$

$$\dot{f}_m''(\Gamma_m) = \begin{cases} \beta & |\Gamma_m| >= a \\ act_{E\sigma}'(\Gamma_m) & |\Gamma_m| < a \end{cases}$$

Where, $\dot{f}_m'(\Gamma_m)$ signifies the ES function, $\dot{f}_m''(\Gamma_m)$ represents the derivative function, and where a indicates the threshold and β signifies the slope, both parameters are preset.

The classification result is proffered by the FCL. Thereafter, for obtaining a precise result, the loss function (LF) is calculated. The LF is assessed betwixt the actual value (Γ_i) and the predicted value ($\hat{\Gamma}_i$) that is provided as:

$$\lambda_n^{loss} = \sum\left(\Gamma_i - \hat{\Gamma}_i\right)^2 \qquad (4.30)$$

For the optimization of weight function, the re-weighted LF is measured that is offered as:

$$w_n^{(t+1)} = w_n^t + \frac{\eta\nu}{mn}\sum_{i=1}^{m}\sum_{j=1}^{n}\forall_{\phi_j}\wp_{v_j}\forall_{\phi}\wp_i\left(a\lg\left(\theta, D_i^S\right)\right)^T \tag{4.31}$$

Wherein, $w_n^{(t+1)}$ signifies the updated weights, w_n^t implies the current weights, η is a meta objective step size, ν is the weight update step size, $\forall_{\phi_j}\wp_{v_j}$ symbolizes the training feature's validation, $\forall_{\phi}\wp_i$ indicates the validation of the tested features, $a\lg\left(\theta, D_i^S\right)$ demonstrates the weight's gradient descent.

Finally, the misclassification error is lessened by the reweighted loss for the CA enhancement aimed at FVR. Figure 4. 2 exhibits the proposed ES-RwCNN's overall outline in pseudo-code.

Input: Extracted features $F_{EXT}^{'} = \left[\xi_1^+, \xi_2^+, \xi_3^+, \xi_4^+, \ldots..\xi_N^+\right]$
Output: Finger Vein Recognition (authorized person or unauthorized person)

Begin
  Initialize the kernel (K_m^l), bias ($\mathrm{B}_{i,j}^l$), pooling layer ($\forall_{layers}^+$), weights $w_{i,j}^l$
  For κ features in dataset
    Evaluate the convolution operation using,
      $\hat{\lambda}_n^l(\kappa) = \sum_{i=0}^{n}\sum_{j=0}^{n} w_{i,j}^l \Gamma_{i,j}^l + \mathrm{B}_{i,j}^l$
    Compute the convolution layer with activation function
      $\hat{\lambda}_n^l = act_{relu}\left(\sum_{i=0}^{N}\sum_{j=0}^{N} w_{i,j}^l \Gamma_{i,j}^l + \mathrm{B}_{i,j}^l\right)$
    Generate pooling layer,
      $\lambda_n^p = \forall_{layers}^+\left(\left|\Gamma_m^l\right|\right)$
    Evaluate the fully connected layer using,
      $\Theta_m^l = act_{E\sigma}\left(\sum_{i=1}^{n} w_i \Im_{i,j} + \mathrm{B}_{i,j}\right)$
    If $\left(\sum\left(\Gamma_i - \hat{\Gamma}_i\right)^2 = 0\right)$
      Accurate finger vein recognition
      If $\left(\hat{\Gamma}_i > 0.5\right)$
        Output as Authorized person
      Else
        Output as Unauthorized person
      End if
    Else
      Update weights using,
        $w_n^{(t+1)} = w_n^t + \frac{\eta\nu}{mn}\sum_{i=1}^{m}\sum_{j=1}^{n}\forall_{\phi_j}\wp_{v_j}\forall_{\phi}\wp_i\left(a\lg\left(\theta, D_i^S\right)\right)^T$
    End if
  End for
End begin

***Figure 4.2*: Pseudo code for proposed ES-RwCNN**

4.8 Results and Discussion

Centered on different performance metrics for the FVR, the complete analysis of the proposed framework's final outcome with prevailing methods is elucidated here. For stating the proposed method's efficiency, both the performance analysis and also comparative analysis are executed. The proposed technique is implemented in MATLAB with machine configuration of Intel core i7 processor, 3.20 GHz CPU Speed, windows 7 OS. The data are amassed from the openly accessible dataset.

4.81 Performance Analysis

Centered upon different evaluation metrics, the proposed work's brief analysis was executed. Besides, a comparative review is also conducted. For the pre-processing model TMF-CLAHE and also the classification model ES-RwCNN, the analysis is executed.

4.82 Performance Analysis of Proposed Pre-processing Technique

Concerning disparate performance metrics, like Correlation, Image Quality Index (IQI), and Spearman Rank Correlation (SRC) with different prevailing methods like CLAHE, Histogram Equalization (HE), and Bi-lateral filtering method, the proposed TMF-CLAHE's performance analysis is validated. Next, for illustrating its efficiency, a comparative study was conducted. Table 4.1 tabulates the metric's evaluation. The performance analysis concerning the proposed TMF-CLAHE's correlation, IQI, and also SRC with different existent techniques, namely CLAHE, HE, and Bi-lateral filtering technique is assessed in table 4.1.

Table 4.1: Performance analysis of proposed TMF-CLAHE based on Correlation, Image Quality Index, and Spearman Rank Correlation

Performance metrics/Techniques	**Correlation**	**Image Quality Index**	**Spearman Rank Correlation**
Proposed TMF-CLAHE	0.971	0.799	0.998
CLAHE	0.940	0.583	0.939
Histogram Equalization	0.850	0.036	0.888
Bi-lateral Filtering	0.941	0.000	0.940

The similarities betwixt the EI and the OI are denoted by correlation. The similarities betwixt the EI and the OI with minimum information loss are denoted by the higher correlation rate. As per that, 0.971 correlations betwixt the images are attained by the proposed TMF-CLAHE, while the existing method obtains a 0.91 average correlation, which is moderately less as analogized to the existent techniques. Furthermore, the SRC is also deemed. The degree of association betwixt the EI and the OI is quantified by the SRC. The higher Spearman correlation characterizes the better model and also vice versa. Thus, a higher SRC of 0.998 is displayed by the TMF-CLAHE proposed, but the prevailing methods acquire an average of 0.922 SRC, which is moderately less when weighted against the proposed one. Therefore, the proposed TMF-CLAHE is more effectual, together with the image is delivered at the higher-quality index at the rate of 0.799, whilst 0.583, 0.036, and 0.000 are attained by the prevailing techniques, like CLAHE, HE, and also Bi-lateral filtering technique correspondingly. Therefore, a quality image with no distortion is offered by the proposed TMF-CLAHE.

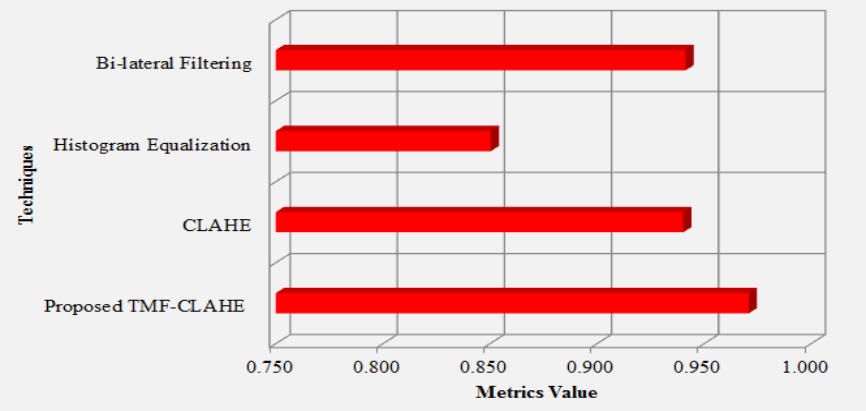

(a)

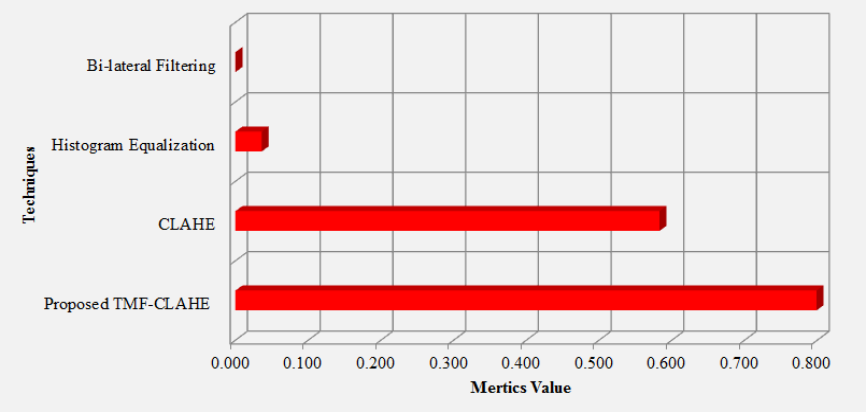

(b)

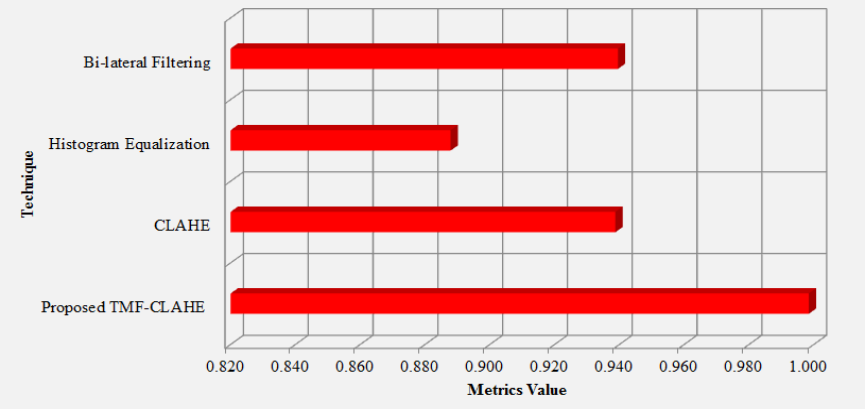

(c)

***Figure 4.3*: Graphical Demonstration of proposed TMF-CLAHE based on (a) Correlation, (b) Image Quality Index and (c) Spearman Rank Correlation**

Figure 4.3 demonstrates the proposed TMF-CLAHE's graphical analysis with different existing methods namely CLAHE, HE, and the Bi-lateral filtering technique. It is obviously

known from figure 4.3 that a greater range of correlation, IQI, and SRC is attained by the TMF-CLAHE. The proposed method's high correlation is shown in figure 4.3 (a); thus, the uneven detection could be effortlessly rectified. Figure 4.3 (b) exhibits the IQI, which assists in clear image delivery. The SRC is exhibited in figure 4.3 (c), which offers a precise association rate. These metrics measure the proposed TMF-CLAHE's effectiveness. Thus, the proposed TMF-CLAHE surpasses the existing technique.

4.83 Performance Analysis of Proposed Classification Technique:

Concerning disparate performance metrics, namely specificity, sensitivity, accuracy, Negative Predictive Value (NPV), recall, precision, F-Measure, Matthews Correlation Coefficient (MCC), FPR, and FRR, the proposed ES-RwCNN's performance analysis is validated. Afterward, a comparative study is conducted with prevailing methods, like Deep NN (DNN), Convolutional DNN (CDNN), along with Artificial NN (ANN). Table 4.2, 4.3, and also 4.4 tabularizes the metric's evaluation.

Table 4.2: Performance analysis of proposed ES-RwCNN based on sensitivity, specificity, accuracy, and NPV

Performance metrics/Techniques	Sensitivity	Specificity	Accuracy	NPV
Proposed ES-RwCNN	97.64	96.46	97.05	97.61
DNN	88.21	84.67	86.44	87.78
CDNN	90.57	91.75	91.16	90.68
ANN	69.81	42.22	56.01	58.31

Table 4.2 illustrates the different performance metrics' analysis, like specificity, NPV, accuracy, and also sensitivity of the ES-RwCNN proposed with the various prevailing techniques, like DNN, CDNN, and ANN. The evaluation metrics must stand with a greater metrics rate for alleviating the VG issue within the network. According to that, the ES-

RwCNN proposed attaining the sensitivity, specificity, accuracy, and NPV at the rate of 97.64%, 96.46%, 97.05%, and 97.61% correspondingly, which overall ranges betwixt 96.46% to 97.64%. However, the metrics' value that overall ranges between 42.22%-91.75% are attained by the prevailing techniques, like DNN, CDNN, and ANN, which is relatively low when weighted against the proposed ES-RwCNN. Hence, the authorized along with the unauthorized person are efficiently distinguished by employing the proposed ES-RwCNN in the FVR.

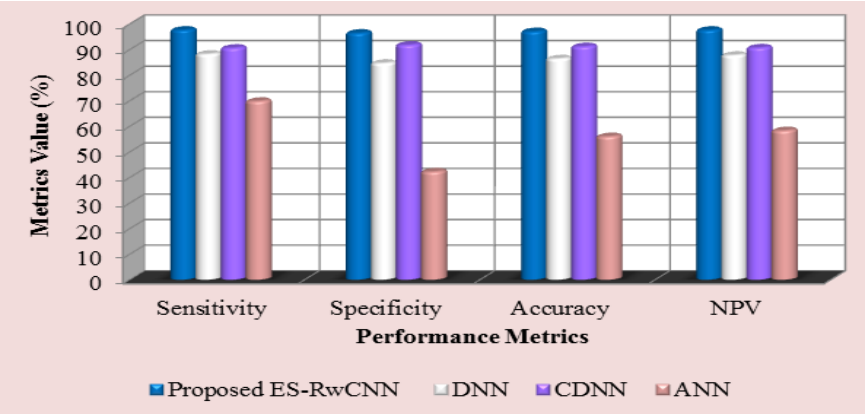

***Figure 4.4*: Graphical representation of the proposed ES-RwCNN based on sensitivity, specificity, accuracy, and NPV**

Figure 4.4 exhibits the graphical depiction of the proposed ES-RwCNN's performance analysis with the disparate prevailing techniques, namely DNN, CDNN, and ANN. It is evidently known as of the figure 4.4 that a superior performance metrics value is gained by means of the proposed one. Thus, the proposed ES-RwCNN surpasses several prevailing ones and offers precise FVR in disparate situations.

Grounded upon the metrics of precision, recall, along with F-Measure, table 4.3 exhibits the proposed ES-RwCNN's evaluation. These metrics are mainly significant in the LF's prediction. The misclassification error is lessened by the LF for the CA enhancement for

***Table 4.3*: Performance analysis of proposed ES-RwCNN based on precision, recall and F-Measure**

Performance metrics/Techniques	Precision	Recall	F-Measure
proposed ES-RwCNN	96.5	97.64	97.07
DNN	85.19	88.21	86.67
CDNN	91.65	90.57	91.1
ANN	54.71	69.81	61.35

FVR. It is depicted as of the table 4.3 that 96.5% precision, 97.64% recall, and 97.07% F-Measure are attained by the ES-RwCNN proposed, which is relatively larger analogized to the prevalent technique. Thus, the existent method, like DNN, CDNN, and ANN attains the metrics' value that overall ranges from 54.71%-91.65%. Therefore, the FV is detected by the proposed one by overcoming the uncertainties along with a reduced error rate as contrasted to the prevailing model.

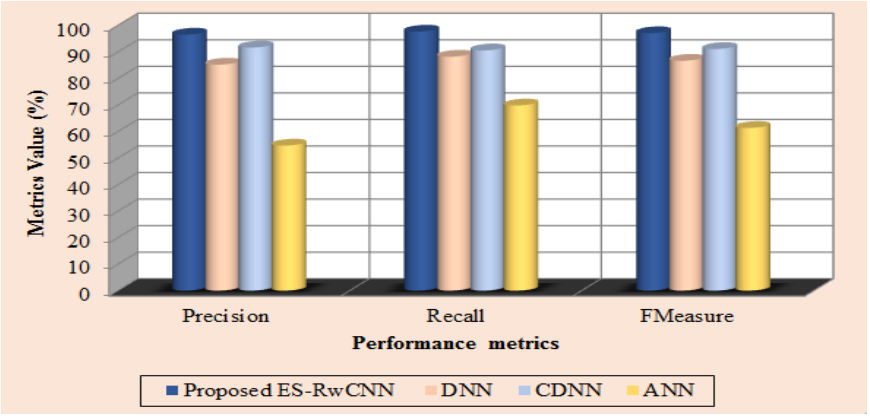

***Figure 4.5*: Graphical representation of the proposed ES-RwCNN based on precision, recall, and F-Measure**

The graphical illustration, which relatively examines the proposed ES-RwCNN with the prevailing methods say DNN, CDNN, and ANN is exhibited in figure 4.5. The proposed ES-RwCNN is more effectual when contrasted to the prevalent methods as stated by the comparative study. Hence, the uncertainties with the decreased error rate are effectively

addressed by the proposed ES-RwCNN whilst the existing technique failed to manage such uncertainties.

Table 4.4: Evaluation of proposed ES-RwCNN based on MCC, FPR, and FRR

Performance metrics/Techniques	**MCC**	**FPR**	**FRR**
Proposed ES-RwCNN	94.11	3.53	2.35
DNN	72.92	15.33	11.79
CDNN	82.32	8.25	9.43
ANN	12.51	57.78	30.18

Centered upon the metrics of MCC, FPR, and FRR, table 4.4 depicts the proposed ES-RwCNN's performance analysis. The misclassification or miss-prediction error that happens in the FV's recognition is efficiently rejected by the lesser value of FPR and FRR. As per that, 3.53% FPR and 2.35% FRR are attained by the proposed one correspondingly. Contrarily, the high prediction rate is attained by the existing technique like DNN, CDNN, and ANN. FPR and FRR's average is 27.12% and 17.13%, correspondingly. Besides that, centered on MCC, the proposed ES-RwCNN is also deemed. The model's success is signified by a higher MCC score. Thus, the high MCC score of 94.11% is attained by the ES-RwCNN proposed, whilst the prevailing technique acquires the MCC score at an average of 60%. Hence, the slow convergence of triplet loss is conquered by the ES-RwCNN proposed and also assures the full usage of information with labels.

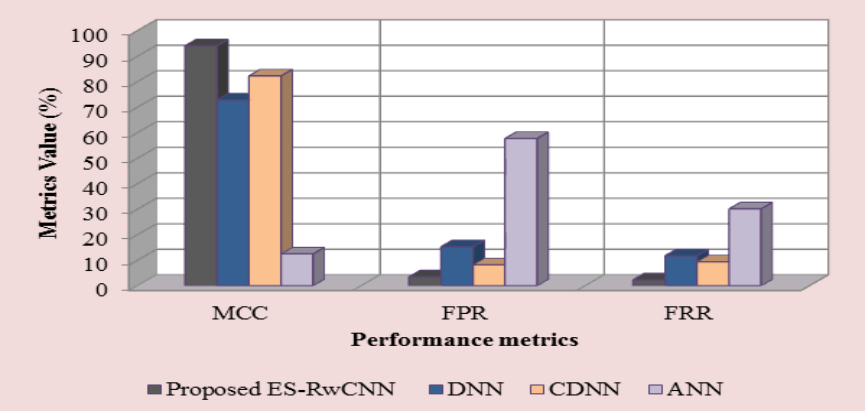

***Figure 4.6*: Graphical analysis of the proposed ES-RwCNN based on MCC, FPR, and FRR**

The proposed ES-RwCNN's detailed analysis with different existing techniques, namely DNN, CDNN, and ANN is proffered in figure 4.6. The best model is proffered by the illustration via examining the false prediction values. The false prediction is lessened by the proposed one and improvises the classification rate by evading misclassification and stays effective against the prevalent methods. Therefore, by attaining lower false prediction values and higher MCC scores, the proposed ES-RwCNN surpasses the prevailing methods.

4.9 Significant Finding

In this proposed work FV image is enhanced by the TMF-CLAHE technique that overcome the illumination variations or uneven shading, vein deformation caused by the finger or vein posture. Over and under enhancement issues are controlled by this technique. The enhanced image have more information content and thus more informative features can be extracted. The proposed Finger Vein recognition has an improved higher accuracy or recognition rate (RR).

AWM-WOA was applied for selecting the most knowledgeable feature from the extracted features, which enhances accuracy and this algorithm also reduces the computation cost

(CC). Finally the proposed technique ES-RwCNN for classification, reduces the classification errors and hence improves accuracy.

This chapter is based on the following work:

Ajai Kumar Gautam & Rajiv Kapoor "*A Novel ES-RwCNN Based Finger Vein Recognition System with Effective L_{12} DTP Descriptor and AWM-WOA Selection"*, Published in Engineering Letters, vol. 30, no.2, pp882-891, 2022 Journal ISSN: 1816-093X / 1816-0948 [SJR-0.265] [ESCI][108]

CHAPTER 5

CONCLUSION AND FUTURE SCOPE

This chapter gives the important conclusions drawn from this research work on the basis of the contributions made either theoretically or experimentally. Further, the details of future work that can be pursued in this research area are given.

5.1 Conclusions

In this research work, two new methods are proposed, one in MMB using two fusion techniques and a deep learning classifier, and the other in the FV recognition system.

In the first method, face, iris, ear, fingerprint, and also front hand are used as the input traits. Herein, the MDLNN classifier is utilized to make the recognition system more robust and also yields greater accuracy (also signified as the recognition rate).

The synthetic dataset is acquired to examine the proposed multi-model BR system's performance, which is analogized with the existent DLNN, CDNN, and ANN techniques regarding the accuracy, precision, recall, F-Measure, sensitivity, specificity, NPV, FPV, FNR, MCC, FRR, and also FDR.

In this examination, the MDLNN proposed yields an efficient outcome analogized to the other classifiers centered on all performance metrics. The proposed MDLNN accuracy is (0.9407), which is greater analogized to every other classifier.

In the second method, FVR is improved by the proposed framework via managing the challenge of unwilling distortions, diagonal pixel information, image variants, etc.

In the TMF-CLAHE technique, the FV gets improved, which concentrates upon irregular shading along with vein posture deformation and enhances the framework's accuracy.

BY utilizing the L_{12}DTP and Edge methods, relevant textural and (Edge Feature) EFs are extracted. Furthermore, AWM-WOA was applied as the 2nd method for selecting the feature, which enhances accuracy along with lessens the CC.

For identifying the FV, the ES-RwCNN classification model is proposed. A low information loss is attained by the framework by attaining a 0.971 correlation betwixt the processed image and OI along with categorizing the FV with 97.05% accuracy and 97.64% sensitivity, as shown by the experimental outcomes. The misclassification is evaded by employing the classification model via obtaining an FPR and FNR of 3.53% and 2.35%, correspondingly, and stays effective when weighted against the prevailing top-notch method.

5.2 Future Research Scope

This research work can be further pursued for MMB recognition to have a more robust, unconstrained recognition system by selecting appropriate biometric traits and by implementing the latest technique to increment the performance and make the system more cost-effective.

In FVR, Combining more than one modality of an individual around the finger, like palm & finger vein, dorsal vein, and fingerprint, will definitely increase recognition performance, but at the computation cost. This computation cost can be optimized.

Further, as these modalities can be captured at the same time, therefore, some of the soft biometrics along with core biometrics can be chosen. Computation costs can be optimized without compromising on accuracy. Also, a new direction has been observed where users can be recognized on the fly with no constraint.

REFERENCES

[1] K. P and T. Thangaraj, "A fast feature selection technique in multi modal biometrics using cloud framework," *Microprocessors and Microsystems*, vol. 79, Nov. 2020, doi: 10.1016/j.micpro.2020.103277.

[2] A. K. Jain, A. Ross, and S. Prabhakar, "An Introduction to Biometric Recognition," *IEEE Transactions on Circuits and Systems for Video Technology*, vol. 14, no. 1, pp. 4–20, Jan. 2004, doi: 10.1109/TCSVT.2003.818349.

[3] A. Iula, "Biometric recognition through 3D ultrasound hand geometry," *Ultrasonics*, vol. 111, Mar. 2021, doi: 10.1016/j.ultras.2020.106326.

[4] B. Sree Vidya and E. Chandra, "Entropy based Local Binary Pattern (ELBP) feature extraction technique of multimodal biometrics as defence mechanism for cloud storage," *Alexandria Engineering Journal*, vol. 58, no. 1, pp. 103–114, Mar. 2019, doi: 10.1016/j.aej.2018.12.008.

[5] A. Iula and M. Micucci, "Multimodal Biometric Recognition Based on 3D Ultrasound Palmprint-Hand Geometry Fusion," *IEEE Access*, vol. 10, pp. 7914–7925, 2022, doi: 10.1109/ACCESS.2022.3143433.

[6] Y. Wang, W. Xie, X. Yu, and L. K. Shark, "An automatic physical access control system based on hand vein biometric identification," *IEEE Transactions on Consumer Electronics*, vol. 61, no. 3, pp. 320–327, Aug. 2015, doi: 10.1109/TCE.2015.7298091.

[7] L. Yang, G. Yang, Y. Yin, and X. Xi, "Finger Vein Recognition with Anatomy Structure Analysis," *IEEE Transactions on Circuits and Systems for Video Technology*, vol. 28, no. 8, pp. 1892–1905, Aug. 2018, doi: 10.1109/TCSVT.2017.2684833.

[8] L. Ma, Y. Wang, and T. Tan, “Iris recognition using circular symmetric filters,” in *Proceedings - International Conference on Pattern Recognition*, 2002, vol. 16, no. 2, pp. 414–417. doi: 10.1109/icpr.2002.1048327.

[9] B. Chanda, Institute of Electrical and Electronics Engineers, Indian Statistical Institute, IEEE Computational Intelligence Society, International Conference on Advances in Pattern Recognition 8 2015.01.04-07 Kolkata, and ICAPR 8 2015.01.04-07 Kolkata, *2015 Eighth International Conference on Advances in Pattern Recognition (ICAPR) 4-7 Jan. 2015, Kolkata, [India]*.

[10] Z. Zhou, E. Y. Du, N. L. Thomas, and E. J. Delp, “A new human identification method: Sclera recognition,” *IEEE Transactions on Systems, Man, and Cybernetics Part A:Systems and Humans*, vol. 42, no. 3, pp. 571–583, May 2012, doi: 10.1109/TSMCA.2011.2170416.

[11] B. Dashtbozorg, A. M. Mendonca, and A. Campilho, “An automatic graph-based approach for artery/Vein classification in retinal images,” *IEEE Transactions on Image Processing*, vol. 23, no. 3, pp. 1073–1083, Mar. 2014, doi: 10.1109/TIP.2013.2263809.

[12] S. Maity and M. Abdel-Mottaleb, “3D ear segmentation and classification through indexing,” *IEEE Transactions on Information Forensics and Security*, vol. 10, no. 2, pp. 423–435, Feb. 2015, doi: 10.1109/TIFS.2014.2379437.

[13] R. Kapoor and P. Mathur, “Face Recognition Using Moments and Wavelets,” vol. 3, pp. 82–95, [Online]. Available: www.ijera.com

[14] S. S. Zhumazhanova, “Biometric Authentication on Thermographic Facial Images Using Neural Network ‘Biometrics-to-Code’ Converter,” 2021. doi: 10.1109/Dynamics52735.2021.9653466.

[15] S. Gutta and Q. Cheng, “Joint Feature Extraction and Classifier Design for ECG-Based Biometric Recognition,” *IEEE Journal of Biomedical and Health Informatics*, vol. 20, no. 2, pp. 460–468, Mar. 2016, doi: 10.1109/JBHI.2015.2402199.

[16] M. Fraschini, A. Hillebrand, M. Demuru, L. Didaci, and G. L. Marcialis, “An EEG-based biometric system using eigenvector centrality in resting state brain networks,” *IEEE Signal Processing Letters*, vol. 22, no. 6, pp. 666–670, Jun. 2015, doi: 10.1109/LSP.2014.2367091.

[17] S. Singh and K. v. Arya, “Key classification: A new approach in free text keystroke authentication system,” 2011. doi: 10.1109/PACCS.2011.5990168.

[18] M. A. Ferrer, M. Diaz-Cabrera, and A. Morales, “Static signature synthesis: A neuromotor inspired approach for biometrics,” *IEEE Transactions on Pattern Analysis and Machine Intelligence*, vol. 37, no. 3, pp. 667–680, Mar. 2015, doi: 10.1109/TPAMI.2014.2343981.

[19] S. B. Sadkhan, B. K. Al-Shukur, and A. K. Mattar, “Human voice extracted biometric features: What can be used for,” in *International Conference on Current Research in Computer Science and Information Technology, ICCIT 2017*, Jun. 2017, pp. 7–12. doi: 10.1109/CRCSIT.2017.7965543.

[20] D. Muramatsu, A. Shiraishi, Y. Makihara, M. Z. Uddin, and Y. Yagi, “Gait-based person recognition using arbitrary view transformation model,” *IEEE Transactions on Image Processing*, vol. 24, no. 1, pp. 140–154, Jan. 2015, doi: 10.1109/TIP.2014.2371335.

[21] K. Gupta, G. S. Walia, and K. Sharma, “Quality based adaptive score fusion approach for multimodal biometric system,” *Applied Intelligence*, vol. 50, no. 4, pp. 1086–1099, Apr. 2020, doi: 10.1007/s10489-019-01579-1.

[22] B. Ammour, L. Boubchir, T. Bouden, and M. Ramdani, "Face–iris multimodal biometric identification system," *Electronics (Switzerland)*, vol. 9, no. 1, Jan. 2020, doi: 10.3390/electronics9010085.

[23] I. Omara, A. Hagag, S. Chaib, G. Ma, F. E. Abd El-Samie, and E. Song, "A Hybrid Approach Combining Learning Distance Metric and DAG Support Vector Machine for Multimodal Biometric System," *IEEE Access*, 2020, doi: 10.1109/ACCESS.2020.3035110.

[24] Milind E. Rane, and Prameya P. Deshpande "Multimodal Biometric Recognition System Using Feature Level Fusion " 2018 Fourth International Conference on Computing Communication Control and Automation (ICCUBEA) IEEE.

[25] H. Mehraj, A. H. Mir, H. Mehraj, and A. H. Mir, "Feature vector extraction and optimisation for multimodal biometrics employing face, ear and gait utilising artificial neural networks," 2009.

[26] J. Raja, K. Gunasekaran, and R. Pitchai, "Prognostic evaluation of multimodal biometric traits recognition based human face, finger print and iris images using ensembled SVM classifier," *Cluster Computing*, vol. 22, pp. 215–228, Jan. 2019, doi: 10.1007/s10586-018-2649-2.

[27] M. A. M. El-Bendary, H. Kasban, A. Haggag, and M. A. R. El-Tokhy, "Investigating of nodes and personal authentications utilizing multimodal biometrics for medical application of WBANs security," *Multimedia Tools and Applications*, vol. 79, no. 33–34, pp. 24507–24535, Sep. 2020, doi: 10.1007/s11042-020-08926-2.

[28] S. Dargan and M. Kumar, "A comprehensive survey on the biometric recognition systems based on physiological and behavioral modalities,"

Expert Systems with Applications, vol. 143. Elsevier Ltd, Apr. 01, 2020. doi: 10.1016/j.eswa.2019.113114.

[29] Swati K. Choudhary, and Ameya K. Naik "Multimodal Biometric Authentication with Secured Templates – A Review", *Proceedings of the International Conference on Trends in Electronics and Informatics (ICOEI 2019) : 23-25, April 2019*.

[30] Aman Kathed, and "et al." "An Enhanced 3-Tier Multimodal Biometric Authentication" *International Conference on Computer Communication and Informatics : January 23-25, 2019, Coimbatore, India*.

[31] R. Chlaoua, A. Meraoumia, K. E. Aiadi, and M. Korichi, "Deep learning for finger-knuckle-print identification system based on PCANet and SVM classifier," *Evolving Systems*, vol. 10, no. 2, pp. 261–272, Jun. 2019, doi: 10.1007/s12530-018-9227-y.

[32] R. Karthiga and S. Mangai, "Feature Selection Using Multi-Objective Modified Genetic Algorithm in Multimodal Biometric System," *Journal of Medical Systems*, vol. 43, no. 7, Jul. 2019, doi: 10.1007/s10916-019-1351-0.

[33] Yan Tong and "et al." "Improving Biometric Identification Through Quality-based Face and Fingerprint Biometric Fusion" *Computer Vision and Pattern Recognition Workshops (CVPRW), 2010 IEEE Computer Society Conference on : date, 13-18 June 2010*. IEEE, 2010.

[34] A. Prakash, R. Krishnaveni, and R. Dhanalakshmi, "Continuous user authentication using multimodal biometric traits with optimal feature level fusion," 2020.

[35] E. mehdi Cherrat, R. Alaoui, and H. Bouzahir, "A multimodal biometric identification system based on cascade advanced of fingerprint, fingervein

and face images," *Indonesian Journal of Electrical Engineering and Computer Science*, vol. 17, no. 3, p. 1562, Mar. 2020, doi: 10.11591/ijeecs.v17.i3.pp1562-1570.

[36] M. Gayatri, U. Bokade, and R. D. Kanphade, "SECURE MULTIMODAL BIOMETRIC AUTHENTICATION USING FACE, PALMPRINT AND EAR: A FEATURE LEVEL FUSION APPROACH."

[37] H. Ma and S. Y. Zhang, "Contactless finger-vein verification based on oriented elements feature," *Infrared Physics and Technology*, vol. 97, pp. 149–155, Mar. 2019, doi: 10.1016/j.infrared.2018.12.021.

[38] R. R. O. Al-Nima, M. A. M. Abdullah, M. T. S. Al-Kaltakchi, S. S. Dlay, W. L. Woo, and J. A. Chambers, "Finger texture biometric verification exploiting Multi-scale Sobel Angles Local Binary Pattern features and score-based fusion," *Digital Signal Processing: A Review Journal*, vol. 70, pp. 178–189, Nov. 2017, doi: 10.1016/j.dsp.2017.08.002.

[39] J. da Wu and C. T. Liu, "Finger-vein pattern identification using principal component analysis and the neural network technique," *Expert Systems with Applications*, vol. 38, no. 5, pp. 5423–5427, May 2011, doi: 10.1016/j.eswa.2010.10.013.

[40] S. Qiu, Y. Liu, Y. Zhou, J. Huang, and Y. Nie, "Finger-vein recognition based on dual-sliding window localization and pseudo-elliptical transformer," *Expert Systems with Applications*, vol. 64, pp. 618–632, Dec. 2016, doi: 10.1016/j.eswa.2016.08.031.

[41] H. Qin, X. He, X. Yao, and H. Li, "Finger-vein verification based on the curvature in Radon space," *Expert Systems with Applications*, vol. 82, pp. 151–161, Oct. 2017, doi: 10.1016/j.eswa.2017.03.068.

[42] K. Su *et al.*, "Human identification using finger vein and ECG signals," *Neurocomputing*, vol. 332, pp. 111–118, Mar. 2019, doi: 10.1016/j.neucom.2018.12.015.

[43] E. C. Lee and K. R. Park, "Image restoration of skin scattering and optical blurring for finger vein recognition," *Optics and Lasers in Engineering*, vol. 49, no. 7, pp. 816–828, Jul. 2011, doi: 10.1016/j.optlaseng.2011.03.004.

[44] S. Li, B. Zhang, L. Fei, and S. Zhao, "Joint discriminative feature learning for multimodal finger recognition," *Pattern Recognition*, vol. 111, Mar. 2021, doi: 10.1016/j.patcog.2020.107704.

[45] K. Su, G. Yang, L. Yang, D. Li, P. Su, and Y. Yin, "Learning binary hash codes for finger vein image retrieval," *Pattern Recognition Letters*, vol. 117, pp. 74–82, Jan. 2019, doi: 10.1016/j.patrec.2018.12.006.

[46] H. Liu, G. Yang, L. Yang, and Y. Yin, "Learning personalized binary codes for finger vein recognition," *Neurocomputing*, vol. 365, pp. 62–70, Nov. 2019, doi: 10.1016/j.neucom.2019.07.057.

[47] F. Liu, G. Yang, Y. Yin, and S. Wang, "Singular value decomposition based minutiae matching method for finger vein recognition," *Neurocomputing*, vol. 145, pp. 75–89, Dec. 2014, doi: 10.1016/j.neucom.2014.05.069.

[48] W. Kang, X. Chen, and Q. Wu, "The biometric recognition on contactless multi-spectrum finger images," *Infrared Physics and Technology*, vol. 68, pp. 19–27, 2015, doi: 10.1016/j.infrared.2014.10.007.

[49] R. V. Adiraju, K. K. Masanipalli, T. D. Reddy, R. Pedapalli, S. Chundru, and A. K. Panigrahy, "An extensive survey on finger and palm vein recognition system," in *Materials Today: Proceedings*, 2021, vol. 45, pp. 1804–1808. doi: 10.1016/j.matpr.2020.08.742.

[50] X. Meng, J. Zheng, X. Xi, Q. Zhang, and Y. Yin, "Finger vein recognition based on zone-based minutia matching," *Neurocomputing*, vol. 423, pp. 110–123, Jan. 2021, doi: 10.1016/j.neucom.2020.10.029.

[51] J. da Wu and C. T. Liu, "Finger-vein pattern identification using SVM and neural network technique," *Expert Systems with Applications*, vol. 38, no. 11, pp. 14284–14289, Oct. 2011, doi: 10.1016/j.eswa.2011.05.086.

[52] D. Zhao, H. Ma, Z. Yang, J. Li, and W. Tian, "Finger vein recognition based on lightweight CNN combining center loss and dynamic regularization," *Infrared Physics and Technology*, vol. 105, Mar. 2020, doi: 10.1016/j.infrared.2020.103221.

[53] Y. Fang, Q. Wu, and W. Kang, "A novel finger vein verification system based on two-stream convolutional network learning," *Neurocomputing*, vol. 290, pp. 100–107, May 2018, doi: 10.1016/j.neucom.2018.02.042.

[54] A. H. Mohsin *et al.*, "Based blockchain-PSO-AES techniques in finger vein biometrics: A novel verification secure framework for patient authentication," *Computer Standards and Interfaces*, vol. 66, Oct. 2019, doi: 10.1016/j.csi.2019.04.002.

[55] W. You, W. Zhou, J. Huang, F. Yang, Y. Liu, and Z. Chen, "A bilayer image restoration for finger vein recognition," *Neurocomputing*, vol. 348, pp. 54–65, Jul. 2019, doi: 10.1016/j.neucom.2018.06.085.

[56] C. Xie and A. Kumar, "Finger vein identification using Convolutional Neural Network and supervised discrete hashing," *Pattern Recognition Letters*, vol. 119, pp. 148–156, Mar. 2019, doi: 10.1016/j.patrec.2017.12.001.

[57] T. Liu, J. Xie, W. Yan, P. Li, and H. Lu, "Finger-vein pattern restoration with Direction-Variance-Boundary Constraint Search," *Engineering Applications*

of Artificial Intelligence, vol. 46, pp. 131–139, Nov. 2015, doi: 10.1016/j.engappai.2015.09.004.

[58] I. Boucherit, M. O. Zmirli, H. Hentabli, and B. A. Rosdi, "Finger vein identification using deeply-fused Convolutional Neural Network," *Journal of King Saud University - Computer and Information Sciences*, vol. 34, no. 3, pp. 646–656, Mar. 2022, doi: 10.1016/j.jksuci.2020.04.002.

[59] W. Yang, W. Luo, W. Kang, Z. Huang, and Q. Wu, "FVRAS-Net: An Embedded Finger-Vein Recognition and AntiSpoofing System Using a Unified CNN," *IEEE Transactions on Instrumentation and Measurement*, vol. 69, no. 11, pp. 8690–8701, Nov. 2020, doi: 10.1109/TIM.2020.3001410.

[60] N. Hu, H. Ma, and T. Zhan, "Finger vein biometric verification using block multi-scale uniform local binary pattern features and block two-directional two-dimension principal component analysis," *Optik (Stuttg)*, vol. 208, Apr. 2020, doi: 10.1016/j.ijleo.2019.163664.

[61] A. K. Gautam and R. Kapoor, "A review on Finger vein based Recognition," 2021. doi: 10.1109/UPCON52273.2021.9667572.

[62] S. Shazeeda and B. A. Rosdi, "Nearest Centroid Neighbor Based Sparse Representation Classification for Finger Vein Recognition," *IEEE Access*, vol. 7, pp. 5874–5885, 2019, doi: 10.1109/ACCESS.2018.2889506.

[63] H. Qin and P. Wang, "A template generation and improvement approach for finger-vein recognition," *Information (Switzerland)*, vol. 10, no. 4, pp. 1–19, 2019, doi: 10.3390/info10040145.

[64] W. Kang, Y. Lu, D. Li, and W. Jia, "From noise to feature: Exploiting intensity distribution as a novel soft biometric trait for finger vein recognition," *IEEE Transactions on Information Forensics and Security*, vol.

14, no. 4, pp. 858–869, 2019, doi: 10.1109/TIFS.2018.2866330.

[65] Y. Li and M. S. Brown, "Single image layer separation using relative smoothness," *Proceedings of the IEEE Computer Society Conference on Computer Vision and Pattern Recognition*, pp. 2752–2759, 2014, doi: 10.1109/CVPR.2014.346.

[66] L. Yang, G. Yang, K. Wang, H. Liu, X. Xi, and Y. Yin, "Point grouping method for finger vein recognition," *IEEE Access*, vol. 7, pp. 28185–28195, 2019, doi: 10.1109/ACCESS.2019.2901017.

[67] L. Yang, G. Yang, Y. Yin, and X. Xi, "Finger Vein Recognition with Anatomy Structure Analysis," *IEEE Transactions on Circuits and Systems for Video Technology*, vol. 28, no. 8, pp. 1892–1905, 2018, doi: 10.1109/TCSVT.2017.2684833.

[68] A. Kumar and Y. Zhou, "Human identification using finger images," *IEEE Transactions on Image Processing*, vol. 21, no. 4, pp. 2228–2244, 2012, doi: 10.1109/TIP.2011.2171697.

[69] L. Lei, F. Xi, and S. Chen, "Finger-Vein Image Enhancement Based on Pulse Coupled Neural Network," *IEEE Access*, vol. 7, pp. 57226–57237, 2019, doi: 10.1109/ACCESS.2019.2914229.

[70] H. Zhang, S. Li, Y. Shi, and J. Yang, "Graph fusion for finger multimodal biometrics," *IEEE Access*, vol. 7, pp. 28607–28615, 2019, doi: 10.1109/ACCESS.2019.2902133.

[71] S. Li, H. Zhang, Y. Shi, and J. Yang, "Novel local coding algorithm for finger multimodal feature description and recognition," *Sensors (Switzerland)*, vol. 19, no. 9, 2019, doi: 10.3390/s19092213.

[72] H. B. Kekre and V. A. Bharadi, "Fingerprint's core point detection using

orientation field," *ACT 2009 - International Conference on Advances in Computing, Control and Telecommunication Technologies*, pp. 150–152, 2009, doi: 10.1109/ACT.2009.45.

[73] L. Zhang, L. Zhang, D. Zhang, and H. Zhu, "Online finger-knuckle-print verification for personal authentication," *Pattern Recognition*, vol. 43, no. 7, pp. 2560–2571, 2010, doi: 10.1016/j.patcog.2010.01.020.

[74] J. Yang and Y. Shi, "Finger-vein ROI localization and vein ridge enhancement," *Pattern Recognition Letters*, vol. 33, no. 12, pp. 1569–1579, 2012, doi: 10.1016/j.patrec.2012.04.018.

[75] S. Bharathi and R. Sudhakar, "Biometric recognition using finger and palm vein images," *Soft Computing*, vol. 23, no. 6, pp. 1843–1855, 2019, doi: 10.1007/s00500-018-3295-6.

[76] H. Liu, G. Yang, L. Yang, K. Su, and Y. Yin, "Anchor-based manifold binary pattern for finger vein recognition," *Science China Information Sciences*, vol. 62, no. 5, pp. 1–16, 2019, doi: 10.1007/s11432-018-9651-8.

[77] W. You, W. Zhou, J. Huang, F. Yang, Y. Liu, and Z. Chen, "A bilayer image restoration for finger vein recognition," *Neurocomputing*, vol. 348, pp. 54–65, 2019, doi: 10.1016/j.neucom.2018.06.085.

[78] J. M. Song, W. Kim, and K. R. Park, "Finger-Vein Recognition Based on Deep DenseNet Using Composite Image," *IEEE Access*, vol. 7, pp. 66845–66863, 2019, doi: 10.1109/ACCESS.2019.2918503.

[79] N. Hu, H. Ma, and T. Zhan, "Finger vein biometric verification using block multi-scale uniform local binary pattern features and block two-directional two-dimension principal component analysis," *Optik (Stuttg)*, vol. 208, no. September 2019, 2020, doi: 10.1016/j.ijleo.2019.163664.

[80] T. Liu, J. Xie, W. Yan, P. Li, and H. Lu, "Finger-vein pattern restoration with Direction-Variance-Boundary Constraint Search," *Engineering Applications of Artificial Intelligence*, vol. 46, pp. 131–139, 2015, doi: 10.1016/j.engappai.2015.09.004.

[81] R. Wang, G. Wang, Z. Chen, Z. Zeng, and Y. Wang, "A palm vein identification system based on Gabor wavelet features," *Neural Computing and Applications*, vol. 24, no. 1, pp. 161–168, 2014, doi: 10.1007/s00521-013-1514-8.

[82] J. Yang, J. Yang, and Y. Shi, "Finger-vein segmentation based on multi-channel even-symmetric Gabor filters," *Proceedings - 2009 IEEE International Conference on Intelligent Computing and Intelligent Systems, ICIS 2009*, vol. 4, pp. 500–503, 2009, doi: 10.1109/ICICISYS.2009.5357631.

[83] X. Li, J. Ji, Y. Xu, S. He, and Q. Zhou, "Research on Low Contrast Image Enhancement Algorithm," *IEEE Advanced Information Technology, Electronic and Automation Control Conference (IAEAC)*, vol. 2021, pp. 1974–1977, 2021, doi: 10.1109/IAEAC50856.2021.9391127.

[84] J.-D. Wu and S.-H. Ye, "Driver identification using finger–vein patterns with radon transform and neural network.," *Expert Syst. Appl.*, vol. 36, no. 3, pp. 5793–5799, 2009.

[85] S. Ahmad Radzi, M. Khalil-Hani, and R. Bakhteri, "Finger-vein biometric identification using convolutional neural network," *Turkish Journal of Electrical Engineering and Computer Sciences*, vol. 24, no. 3, pp. 1863–1878, 2016, doi: 10.3906/elk-1311-43.

[86] W. T. Dongdong Zhao, Hui Ma, Zedong Yang, Jianian Li, "Finger vein recognition based on lightweight CNN combining center loss and dynamic

regularization," *Infrared Physics & Technology*, vol. 105, 2020.

[87] W. Yang, W. Luo, W. Kang, Z. Huang, and Q. Wu, "FVRAS-Net: An Embedded Finger-Vein Recognition and AntiSpoofing System Using a Unified CNN," *IEEE Transactions on Instrumentation and Measurement*, vol. 69, no. 11, pp. 8690–8701, 2020, doi: 10.1109/TIM.2020.3001410.

[88] I. Boucherit, M. O. Zmirli, H. Hentabli, and B. A. Rosdi, "Finger vein identification using deeply-fused Convolutional Neural Network," *Journal of King Saud University - Computer and Information Sciences*, no. xxxx, 2020, doi: 10.1016/j.jksuci.2020.04.002.

[89] W. K. Yuxun Fang, Qiuxia Wu, "A novel finger vein verification system based on two-stream convolutional network learning," *Neurocomputing*, vol. 290, pp. 100–107, 2018, doi: https://doi.org/10.1016/j.neucom.2018.02.042.

[90] C. Xie and A. Kumar, "Finger vein identification using Convolutional Neural Network and supervised discrete hashing," *Pattern Recognition Letters*, vol. 119, pp. 148–156, 2019, doi: 10.1016/j.patrec.2017.12.001.

[91] R. S. Kuzu *et al.*, "On-the-Fly Finger-Vein-Based Biometric," vol. 15, pp. 2641–2654, 2020.

[92] R. S. Kuzu, E. Maiorana, and P. Campisi, "Loss functions for CNN-based biometric vein recognition," *European Signal Processing Conference*, vol. 2021-Janua, pp. 750–754, 2021, doi: 10.23919/Eusipco47968.2020.9287517.

[93] by P. Abhishek, "Study on Enhancing the accuracy of fingerprint recognition system."

[94] A. Raju, G. S. Dwarakish, and D. V. Reddy, "Modified self - Adaptive Plateau Histogram Equalization with mean threshold for brightness preserving and contrast enhancement," in *2013 IEEE 2nd International Conference on Image*

Information Processing, IEEE ICIIP 2013, 2013, pp. 208–213. doi: 10.1109/ICIIP.2013.6707584.

[95] C. H. Ooi, N. P. Kong, and H. Ibrahim, "Bi-histogram equalization with a plateau limit for digital image enhancement," *IEEE Transactions on Consumer Electronics*, vol. 55, no. 4, pp. 2072–2080, Nov. 2009, doi: 10.1109/TCE.2009.5373771.

[96] S. M. Pizer, R. E. Johnston, J. P. Ericksen, B. C. Yankaskas, and K. E. Muller, "Contrast-limited adaptive histogram equalization: Speed and effectiveness," in *Proceedings of the First Conference on Visualization in Biomedical Computing*, 1990, pp. 337–345. doi: 10.1109/vbc.1990.109340.

[97] Q. Ji and R. Shi, "A novel method of image segmentation using watershed transformation," in *Proceedings of 2011 International Conference on Computer Science and Network Technology, ICCSNT 2011*, 2011, vol. 3, pp. 1590–1594. doi: 10.1109/ICCSNT.2011.6182269.

[98] R. B. Vallabhaneni and V. Rajesh, "BTSWASH: Brain tumour segmentation by water shed algorithm," in *International Conference on Signal Processing and Communication Engineering Systems - Proceedings of SPACES 2015, in Association with IEEE*, Mar. 2015, pp. 366–369. doi: 10.1109/SPACES.2015.7058285.

[99] A. Seal, A. Das, and P. Sen, "Watershed: An Image Segmentation Approach." [Online]. Available: www.ijcsit.com

[100] D. N. Zheng, J. X. Wang, Y. N. Zhao, and Z. H. Yang, "An Iterative Algorithm for KLDA Classifier."

[101] V. Roth and V. Steinhage, "Nonlinear Discriminant Analysis using Kernel Functions."

[102] W. Wu, J. He, and J. Zhang, "A KERNELIZED DISCRIMINANT ANALYSIS ALGORITHM BASED ON MODIFIED GENERALIZED SINGULAR VALUE DECOMPOSITION."

[103] H. Wan, "Deep learning:neural network, optimizing method and libraries review," in *Proceedings - 2019 International Conference on Robots and Intelligent System, ICRIS 2019*, Jun. 2019, pp. 497–500. doi: 10.1109/ICRIS.2019.00128.

[104] International Neural Network Society, E. Verband der Elektrotechnik, and Institute of Electrical and Electronics Engineers., *ANNA '18 ; Advances in Neural Networks and Applications 2018 : 15-17 Sept. 2018.*

[105] M. N. Hoda, *International Conference on Computing for Sustainable Global Development (INDIACom) : 11th to 13th March, 2015, Bharati Vidyapeeth's Institute of Computers, Applications and Management (BVICAM)*.

[106] U. Anitha, S. Malarkkan, J. Premalatha, and V. Manonmani, "Comparison of standard edge detection techniques along with morphological processing and pseudo coloring in sonar image," Oct. 2016. doi: 10.1109/ICETETS.2016.7603057.

[107] A. K. Gautam and R. Kapoor, "Multi-modal biometric recognition system based on FLSL fusion method and MDLNN classifier," 2021.

[108] A. Gautam and R. Kapoor, "A Novel ES-RwCNN Based Finger Vein Recognition System with Effective L12 DTP Descriptor and AWM-WOASelection," *Engineering Letters*, vol. 30, no. 2, pp. 882–891, Jun. 2022, Accessed: May 16, 2022. [Online]. Available: http://www.engineeringletters.com/issues_v30/issue_2/EL_30_2_54.

AUTHOR BIOGRAPHY

Ajai Kumar Gautam,
Assistant Professor,
Department of Electronics & Communication Engineering,
Delhi Technological University, Delhi, India
Email: **ajai.gautam@gmail.com**

Ajai Kumar Gautam received the Bachelor of Technology (B.Tech.) from Harcourt Butler Technological Institute (Now HBTU), Kanpur, U.P, India, in the year 1997 and the Master of Engineering (M.E) from Delhi College of Engineering (Now Delhi Technological University), Delhi, India, in the year 2007. Presently, he is working as an Assistant Professor in the Department of Electronics & Communication Engineering, Delhi Technological University, Delhi, India-110042. His research interests include Biometric Recognition, Pattern Recognition, Image Processing, and Digital system Design.